Spectroscopic studies of microwave plasmas at atmospheric pressure

Diploma paper
by
Mats Fagerström

Lund Reports on Atomic Physics, LRAP-183
Lund, September 1995

Abstract

Emission spectroscopy has been used to study plasmas generated in a microwave cavity at atmospheric pressure. Plasmas were generated in air, nitrogen and different mixtures of helium with air, nitrogen and argon. The spectral components of the emitted radiation have been identified and their relative distribution have, in some cases, been measured. Electron temperatures and vibrational temperatures of molecules have been calculated assuming local thermal equilibrium, LTE, to hold. The not very accurate results yield an electron temperature of about 3400 K, and a gas temperature of about 5000 K, in the studied plasmas. These temperatures indicate that LTE is not valid. Taking the limited line emission obtained in consideration, a corona-like state of equilibrium for the studied plasmas is suggested.

Contents

1 Introduction

During the last decades the field of plasma research has become very large and is today offering an enormous amount of literature treating a wide range of different plasmas. Naturally occurring plasmas are being studied by astrophysicists, whose work are closely related to measurements of atomic parameters in laboratory plasmas. Applications have been found in a wide variety of fields, such as surface treating and nuclear fusion experiments. In surface treating, plasmas are used to change the properties of the surface of a material. This can be done by taking advantage of some plasma properties e.g. heat, radiation or particle flux. Plasmas can also be used to affect a material that is being sprayed on a surface.

Plasmas produced in a laboratory environment, can be classified according to the method of generation, the material from which the plasma was produced and the pressure of the plasma. Plasma generation can be accomplished by using electrical arcs, microwave radiation, inductive coupling, high power laser radiation etc.

In this paper, microwave plasmas at atmospheric pressure have been studied. The used plasma generator has been studied previously, as described in Ref. [1]. The purpose of this work has been to characterize the properties of the plasmas generated by this device, using emission spectroscopy. The study consists of spectral analysis revealing partitioning atoms and molecules and their relative distribution together with efforts to estimate the kinetic temperatures of the plasma particles.

The results of the studies performed within the frame of this work may give rise to more questions than answers. No method for temperature determinations for the assumed actual state of equilibrium has been used, which limits the importance of the evaluated temperatures. Due to limitations in the spectroscopic equipment and lack of control of the plasma generation, systematic measurements have been difficult to perform. Variations in the plasma parameters over time and in different parts of the plasmas have therefore not been investigated.

2 Basic properties of plasma physics

2.1 Introduction

Plasma is regarded as the fourth state of matter. About 99% of all matter in the Universe, whether as stellar, interstellar or intergalactic material, is plasma. Plasma is a gas that is completely or partially ionized through energy absorption - heating. A plasma is thus a mixture of negatively charged electrons, positive ions and neutral atoms. The total system is assumed to be neutral. As the ions and atoms are much heavier than the electrons, yielding a lower thermal velocity, the kinetics of a plasma can often be described by the motion of the electron gas relative the ions and atoms. Two parameters of interest for a plasma are the electron density, n_e, and the kinetic electron temperature, T_e. This temperature can be expressed in units of K as well as eV. A more strict definition of the plasma parameters, as moments of the distribution functions of the electrons and other particles, is found in Ref. [2].

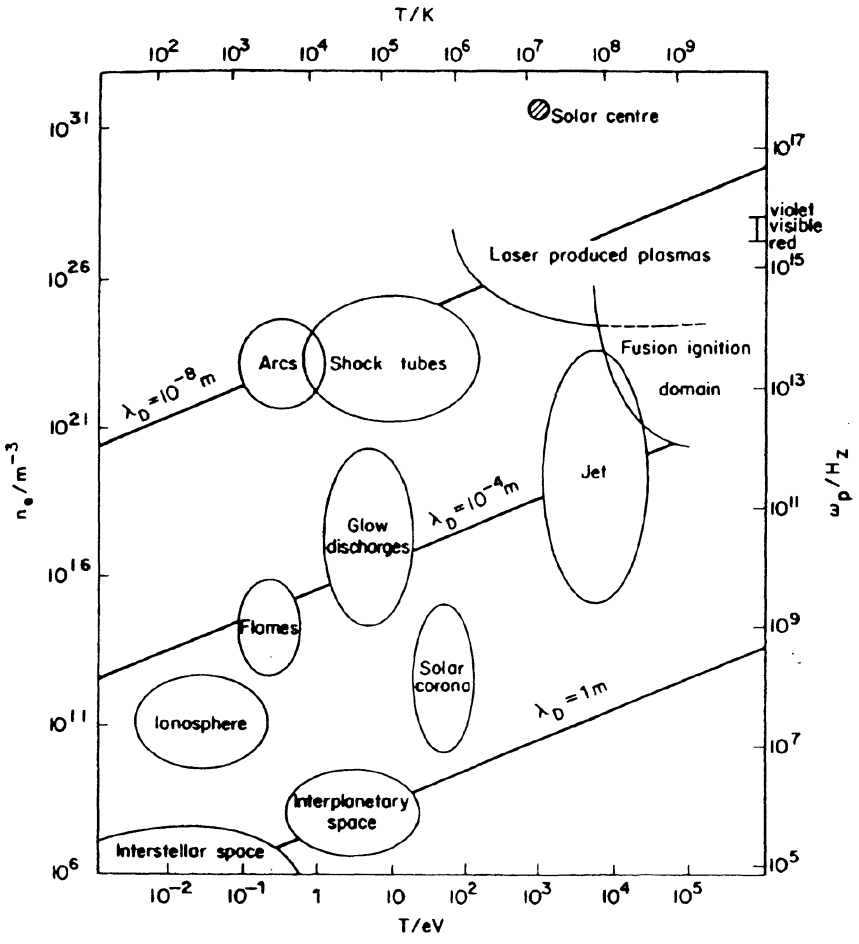

Fig. 2.1 *Different plasmas for varying electron density and temperature [3].*

The kinetic energy of the electrons, kT_e with k being the Boltzmann constant, in an electrical field, is related to their velocity by the Maxwellian velocity distribution [4]

$$n(v) = n_e v^2 \sqrt{\frac{2}{\pi}} \left(\frac{m_e}{kT_e} \right)^{3/2} e^{-\frac{m_e v^2}{2kT}}, \tag{2.1}$$

where $n(v)$ is the density of electrons with the velocity v, e is the elementary charge and m_e is the electron mass. Fig. 2.1 shows some typical plasmas at different conditions. The electron density and the electron temperature can vary over an enormous range. In the diagram also the Debye length, λ_D, and the plasma frequency, ω_{pe}, are included. These parameters are defined in Eqs. (2.2) and (2.10).

Compared with the forces between neutral particles in an ideal gas, the Coulomb-forces between charged particles in a plasma are strong and long-ranged. This will lead to a coupling between the particles so that collective effects will dominate the behaviour of a plasma. If a new charged particle is inserted it will give rise to a potential distribution that decreases faster than the Coulomb potential; the particle, a local disturbance, will be shielded. The distance at which the local effect of the disturbance can no longer be obtained is called the Debye length, and it can be calculated to be (in metres) [3]

$$\lambda_D = \sqrt{\frac{\varepsilon_0 kT_e}{n_e e^2}}. \tag{2.2}$$

Here ε_0 is the permittivity constant of vacuum. Eq. (2.2) above only takes the electrons into consideration. The collective effects of this medium, caused by Coulomb-interactions between the free electrons, may be regarded as the basic criterion of a plasma. The dimension of a plasma, L, must then be much greater than the Debye length; i.e. $L >> \lambda_D$, if collective effects are to dominate.

2.2 Atomic Processes

At the basis of all collective effects are the atomic processes by which electrons, ions and photons interact. To understand an emission spectrum of a plasma, these processes must be considered. The energies of the atoms and ions[1] in a plasma are changed through collisions with electrons or by interaction with photons. The atoms can in these processes either gain or loose energy. The basic atomic processes occurring between two bound states in an atom are illustrated in Fig. 2.2.

1. In this section, as in the following ones, often only the atoms will be discussed, but the discussion will be valid for the ions as well. An important thing to remember, however, is that the ions are charged and thus will interact with other ions, forming an ion gas, which in turn will interact with the electron gas, all due to the Coloumb-forces.

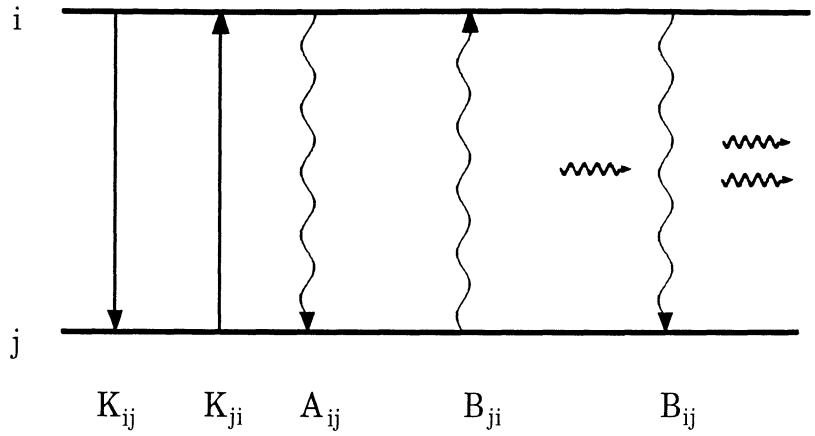

Fig. 2.2 *Electron transitions between two bound states in an atom. K is collisional transitions, A_{ij} is spontaneous deexcitations, B_{ji} is absorption and B_{ij} is stimulated emission.*

Through electron-impact collisions atoms are excited or deexcited. The probability for this non-radiating transition to take place, from state i to j, is here written as K_{ij}. This collision rate is often written as $\langle \sigma_{ij} v \rangle$, where σ_{ij} is the cross section for the process $i \rightarrow j$ and v is the velocity of the electrons.

An excited electronic level has a finite lifetime. The atom will thus be deexcited by spontaneously emitting a photon, if the atom is undisturbed for this time range. A_{ij} is the spontaneous atomic transition probability.

The radiation in a plasma can be absorbed ($j \rightarrow i$) or lead to stimulated emission ($i \rightarrow j$). The latter means that one incoming photon will result in two outgoing photons. The probability for any of these transitions is found to be $B\rho(\upsilon)$, where $\rho(\upsilon)$ is the radiation density for the frequency υ corresponding to the transition energy $hc\upsilon$, where h is Planck's constant and c the speed of light. The atomic constants A and B are often referred to as the Einstein coefficients.

If the gained energy in an atomic process is large enough, the atom will be ionized; an electron is then excited from a bound level in an atom to a free state in the electron gas. The ionization energy is the energy necessary to ionize an atom in the ground state. The difference between the energy needed to ionize an atom, in any state, and the energy that is actually gained, e.g. in an electron-impact collision, will be the resulting kinetic energy of the free electron. The inverse of ionization is called recombination; the excess energy is, in this process, emitted as a photon. Recombination results in an unstructured continuous spectrum. The ionization rate and the recombination rate have to be balanced if the electron density will remain constant.

Bremsstrahlung occurs when a free electron is accelerated by an electric field, for instance in an interaction with an atom. The loss in kinetic energy is then transformed into radiation energy. Bremsstrahlung is a transition between two free electron states, and the spectrum will be continuous.

2.3 Equilibria

To be able to predict the radiating behaviour of any atomic species in a plasma, one must know the expected population of its various possible states. This dependence is governed by the Boltzmann distribution and can be seen in Eq. (3.1). The relative population in any given quantum state, with energy E, can under thermodynamic equilibrium be calculated to be, with n_n being the density of the state n [5]

$$\frac{n_n}{n} = \frac{g_n \exp(-E_n / kT)}{\sum_j g_n \exp(-E_n / kT)} \equiv \frac{g_n \exp(-E_n / kT)}{u(T)}. \tag{2.3}$$

In the expression at the right hand side the numerator is the Boltzmann factor, while the denominator $u(T)$ is called the partition function. g_n is the statistical weight for the state n, i.e. the number of such states. The theory can be extended to atoms of subsequent ionization. Consider the ground state of an ion (or atom) with charge z, and a state n with charge $z-1$ and the ionization energy χ. The ratio of the densities of these states is then given by the following relation, which is a form of the Saha-equation,

$$\frac{n_e n_1^z}{n_n^{z-1}} = \frac{2g_1^z}{g_n^{z-1}} \left(\frac{m_e kT}{2\pi\hbar^2} \right)^{3/2} e^{-\frac{\chi}{kT}}. \tag{2.4}$$

In this equation is used $\hbar = h/2\pi$. The change in the population of a state i can be written as a differential equation of the atomic processes explained in the former section. If we also consider levels above i, the relation is

$$\frac{dn_i}{dt} = -\sum_{j \neq i} \left[n_i A_{ij} - n_j A_{ji} + (n_i B_{ij} - n_j B_{ji}) \rho(\upsilon) + n_e n_i \langle \sigma_{ij} v \rangle - n_e n_j \langle \sigma_{ji} v \rangle \right]. \tag{2.5}$$

At steady-state $dn_i/dt = 0$ and some kind of equilibrium is established. It could then be possible to predict the emission spectrum if all processes were known. The problem is, however, very complex and simplified models have to be used.

2.3.1 Thermal equilibrium

For a plasma in thermal equilibrium the following conditions are satisfied:

i) All particles obey the Maxwell velocity distribution.
ii) The energy levels in the atoms are populated in accordance to the Boltzmann distribution.
iii) The distribution between different stages of ionization for any species is given by the Saha-equation.

iv) The intensity distribution of the radiation, $\rho(\upsilon)$, follows the Planck formula[2], i.e. the plasma can be considered as a blackbody radiator.

All these distributions will be functions of the system temperature. If all four conditions are met we have complete thermal equilibrium. The atomic processes are completely cancelled out by their inverses, so that the radiation has no coupling to the atoms. The plasma is radiating as a perfect blackbody and no lines can be seen. This state is very seldom achieved in laboratories. Therefore a less generalised form called local thermal equilibrium, LTE, has been defined. LTE is valid if collisional events dominate over the radiating processes. Condition *iv)* will not hold any longer, but the three first conditions will be valid and they will still determine an unambiguous temperature, which now is the electron temperature T_e. This temperature does not have to be equal to the temperatures of the atoms (the gas temperature), which is related to their velocity distribution. If collisions are to dominate in a plasma, the electron density has to be high. In Ref. [3] the electron density required for collisions to dominate over the radiating processes is given as

$$n_e \geq 1.6 \cdot 10^{18} T_e^{1/2} (\Delta E)^3 \ \mathrm{m}^{-3}. \tag{2.6}$$

ΔE, the energy difference between two levels being studied, and T_e is here in eV. In practice, the electron density should be about 10^{22} m^{-3} [6]. Even LTE is not that easily obtained so one also talks about partial local thermal equilibrium (PLTE). Free and bound-excited electrons are in mutual equilibrium, but not with the ground state [7]. The ground states of the atoms are, relatively speaking, either under- or overpopulated [8].

2.3.2 Coronal equilibrium

The coronal model is valid when the electron density is low. The collision rate will then be low enough for excited states to deexcite by spontaneous radiation. All downward transitions can thus be said to be radiating, while upwards transitions are collisional, essentially from the ground state. The population of an excited state relative the ground state is then obtained from Eq. (2.5) as

$$\frac{n_i}{n_1} = \frac{n_e \langle \sigma_{1i} v \rangle}{\sum_j A_{ij}}. \tag{2.7}$$

Ionization from and recombination to the ground state will be balanced in the same way. The spontaneous transition rate decreases quite rapidly for higher states. It therefore exists a level above which collisional transitions will dominate [2]. The states above this level are approximately in local thermal equilibrium with free electrons and ionized atoms. The Saha-equation will then be obeyed for the higher states.

---

2. The spectral energy density of the radiation per unit volume according to Planck is [6]

$$P(\upsilon, T) = \frac{8\pi h \upsilon^3}{c^3} \frac{1}{e^{h\upsilon/kT} - 1}.$$

2.4 Plasma heating

When heating a plasma, the energy is often transferred from the power source to the electrons. Through electron-impact collisions the energy is then spread to the ions and atoms. The resulting gas temperature of this energy distribution will, however, depend on what particles that interact with the electrons, i.e. what gas that is used as a plasma source. Fig. 2.3 shows that for a given amount of energy being absorbed by a gas, the resulting kinetic temperature is much lower for molecular gases. This is due to the dissociation energy necessary to break the molecular bonds. The initial slope of the curve for argon and helium is equal to 5/2 R, the specific heat of a monoatomic ideal gas, R, being the gas constant [9]. The energy absorption, as a function of the temperature, will increase near the ionization limit for an atomic gas, in the same way as it increases near the dissociation limit for a molecular gas. As can be seen, helium has a higher ionization energy than the other elements in the diagram. A gas can, during the dissociation or ionization phase, absorb a great amount of energy without any significant increase of the gas temperature. It may therefore be, that a gas in these temperature regions, is more stable and less depending on the power of the plasma heating source.

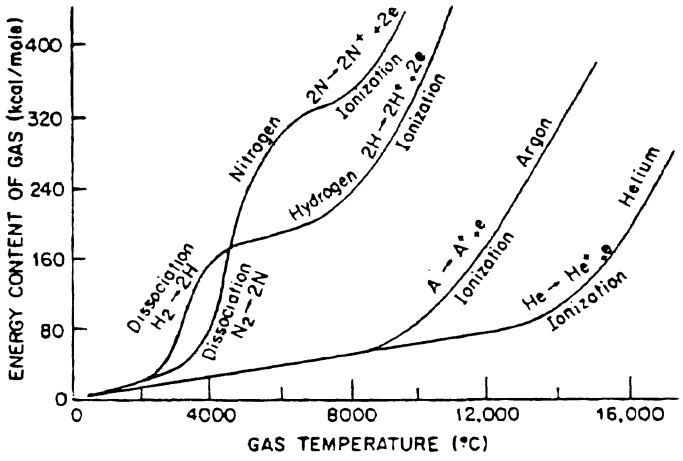

Fig. 2.3 *Energy content of a gas, at atmospheric pressure, as a function of the gas temperature [10].*

2.5 Waves in plasma

In a homogenous plasma both transverse (electromagnetic) and longitudinal (electrostatic) waves can propagate. The latter, plasma oscillation waves, has no analogy in ordinary media and the thermal motions of the particles of the plasma play an essential role. These waves can be compared with an acoustic wave (sound) propagating in a gas through changes in the pressure of the gas. A longitudinal plasma wave will thus transport local variations in the electron density. Detailed treatments of plasma waves and wave propagation in plasmas, including analytical expressions for different incident angels and the

Faraday effect can be found in Refs. [2,11,12,13]. The equations in this section were taken from Ref. [14].

2.5.1 Plasma oscillations

Plasma is a mixture of an electron gas and a gas of heavier ions. If the electrons are displaced , e.g. by compression, relative to the ions, an electrostatic force trying to get the system back to its initial state will arise. The resulting motion will be an oscillation. In the case where the thermal motions of the electrons and ions can be ignored, this can be described by an oscillation at an electron plasma frequency

$$\omega_{pe} = \left(\frac{n_e e^2}{m_e \varepsilon_0} \right)^{\frac{1}{2}}. \tag{2.8}$$

The group velocity $\partial\omega / \partial k$ for such an oscillation is equal to zero, i.e. we have no wave propagation. If the thermal velocity, V_{te}, of the electrons is not negligible, we will get a wave propagating through the plasma as a longitudinal wave fulfilling the dispersion relationship

$$\omega^2 = \omega_{pe}^2 + 3k_\lambda^2 V_{te}^2, \qquad V_{te} = \left(\frac{kT_e}{m_e} \right)^{\frac{1}{2}}, \tag{2.9}$$

where $k_\lambda = 2\pi/\lambda$ is the wave propagation constant.

There may be a net transfer of energy from the wave to the plasma, if the thermal velocity components of the particles match that of the wave. The matching requires that the velocity of the electrons is close to the phase velocity of the wave, $V_p = \omega/k$, and in the same direction. The velocities of the electrons will then get locked to the phase velocity of the wave. If the electrons that increase their velocity are larger in number than the ones having a decreased velocity, the plasma will gain energy from the wave; we thus get Landau damping of the wave. It could also happen that the wave gain energy from the electrons, which will lead to instability [13].

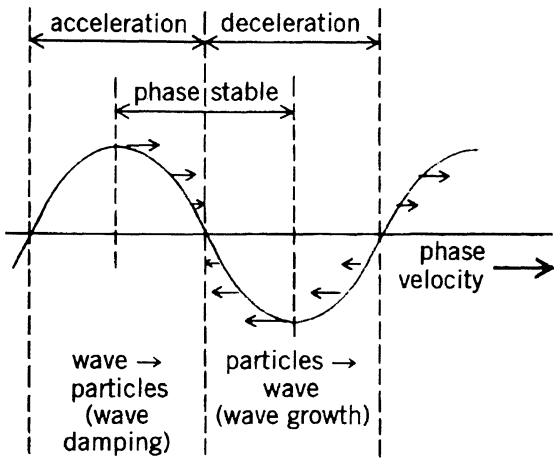

Fig 2.4 *Illustration of wave damping and wave growth. Electrons with a velocity lower than the phase velocity will be accelerated, and electrons with a higher velocity will be decelerated* [*13*].

2.5.2 Electromagnetic wave propagation

For a transverse wave propagating through a plasma, the following dispersion relationship holds

$$\omega^2 = \omega_{pe}^2 + c^2 k_\lambda^2 . \tag{2.10}$$

Propagation will occur if the wave number k_λ is real, i.e. $\omega > \omega_{pe}$. The plasma then behave as a medium with the refractive index less than one. A wave will be reflected when $\omega = \omega_{pe}$; for a given frequency this occurs at the critical density

$$n_c = \frac{\varepsilon_0 m_e \omega^2}{e^2} . \tag{2.11}$$

3 Plasma spectroscopy

3.1 Optical depth

When studying the emission from a plasma, it is important to know if all radiation emitted is detected, or if some part of the radiation is being reabsorbed in the plasma. The optical thickness determines how deep in the plasma we can see. If the plasma is optically thick, all radiation from the centre is self-absorbed and only the boundary can be studied. If practically no absorption take place, the plasma is said to be optically thin. In the latter case, the emission along the line of sight through the plasma is integrated. Calculations of, e.g. T_e from line intensity ratios, would thus reveal the average temperature. The Abel inversion formula [2,15] can be used in order to eliminate the problem of reabsorption for a homogenous plasma of cylindrical symmetry. But this correction is in practice uncertain and thus rather difficult to perform.

3.2 Line radiation

Line radiation originates from a transition between two bound electronic states in an atom or ion. Both the intensity and the broadening of a line will depend on the characteristics of the plasma.

3.2.1 Line intensity

The line intensity is proportional to the number of atoms, N, that are in the upper of the two levels involved in the transition. If the population of the various states are thermal, i.e. follows the Boltzmann distribution, the intensity of a radiating deexcitation, from level i, with the excitation energy E, to level k, is found as [16]

$$I = \frac{N}{u} hc \frac{g_k A_{ki}}{\lambda} e^{-\frac{E}{kT}}. \tag{3.1}$$

This function can be written in an equivalent form, using the absorption oscillator strength, f_{ik}, instead of the spontaneous transition probability. One must then use the statistical weight of the upper level;

$$I = \frac{N}{u} \frac{8\pi^2 e^2 h}{m} \frac{g_i f_{ik}}{\lambda^3} e^{-\frac{E}{kT}}. \tag{3.2}$$

In the literature it is possible to find measured values of the transition probability and the oscillator strength. The accuracy of the tabulated values may, however, be quite limited. They depend on the exact conditions for the actual measurement.

3.2.2 Line broadening

Atomic line radiation will be broadened by various mechanisms. The most fundamental is the natural line width, caused by the finite lifetime of the excited states. The Heisenberg uncertainty principle, $\Delta E \cdot \Delta t \geq \hbar$, provides a lower limit for the line width. Doppler broadening occurs if the radiating atoms are moving along the line of observation when emitting light. The Doppler shift for each such event will be dependent on the velocity of that particular atom. If we have a Maxwellian velocity distribution, the broadening can be formulated as a function of the temperature of the atoms [5]

$$\Delta\upsilon = \frac{2\upsilon_0}{c}\sqrt{\frac{kT_a 2\ln 2}{m_a}}, \tag{3.3}$$

where the undisturbed frequency of the radiation is υ_0 and the temperature and the mass of the emitting atoms are T_a and m_a, respectively.

Various interactions between particles in a plasma will lead to what is summarized as pressure broadening. The strongest of these is the one caused by the Stark effect. An atom or ion in a plasma will be influenced by the electrostatic field caused by the surrounding electrons and ions. The Stark effect will lead to a broadening and a shift of a spectral line as well as a change of the line profile [17]. The effect is quadratic on the field for all elements except for hydrogen, for which it is linear. The Stark effect is depending on the electron density, which has to be rather high, about 10^{18}-10^{20} m^{-3} [15], for Stark broadening to dominate in a plasma. For lower electron densities, Doppler broadening will dominate. The magnitude of the Stark broadening is largest for hydrogen.

3.3 Diatomic molecular structure

The discussion has so far been limited to emission from atoms and ions, but a cold plasma may not contain sufficient energy to break the bonds of molecules, why these will contribute to the emitted radiation. The structure of diatomic molecules is much more complex than for atoms and will not be treated in great detail in this work. Some fundamental properties that explains observed molecular spectra will, however, be briefly described. For a detailed description of molecular structure see Herzberg [18].

Like an atom, a molecule will have specific electronic states. The ground state is designated X, while the excited states are called A, B, C etc. But in addition to the electronic structure, a diatomic molecule can also rotate and vibrate, making the system more complex. The quantum-mechanical picture of the experimental observations include molecular rotation and vibration, yielding additional components to the internal energy on top of the electron energy.

3.3.1 Vibrational energy

Two atoms forming a molecule will vibrate along the internuclear axis. The resulting vibrational energy will split up the electronic states in finer levels. Since the potential curves of the electronic levels are not parabolic, the solution will be an anharmonic oscillator. The energy values of the anharmonic oscillator, relative the non-vibrating state are $E=hcG(v)$, where $G(v)$, in cm^{-1}, is given by

$$G(v) = \omega_e(v+\tfrac{1}{2}) - \omega_e x_e(v+\tfrac{1}{2})^2 + \omega_e y_e(v+\tfrac{1}{2})^3. \qquad (3.4)$$

ω_e, x_e and y_e are molecular constants and v is the vibrational quantum number. The first term in the formula corresponds to a harmonic oscillator. For a harmonic oscillator the energy is equidistant. Any transition is allowed, i.e. there are no restrictions for $\Delta v=v'-v''$.

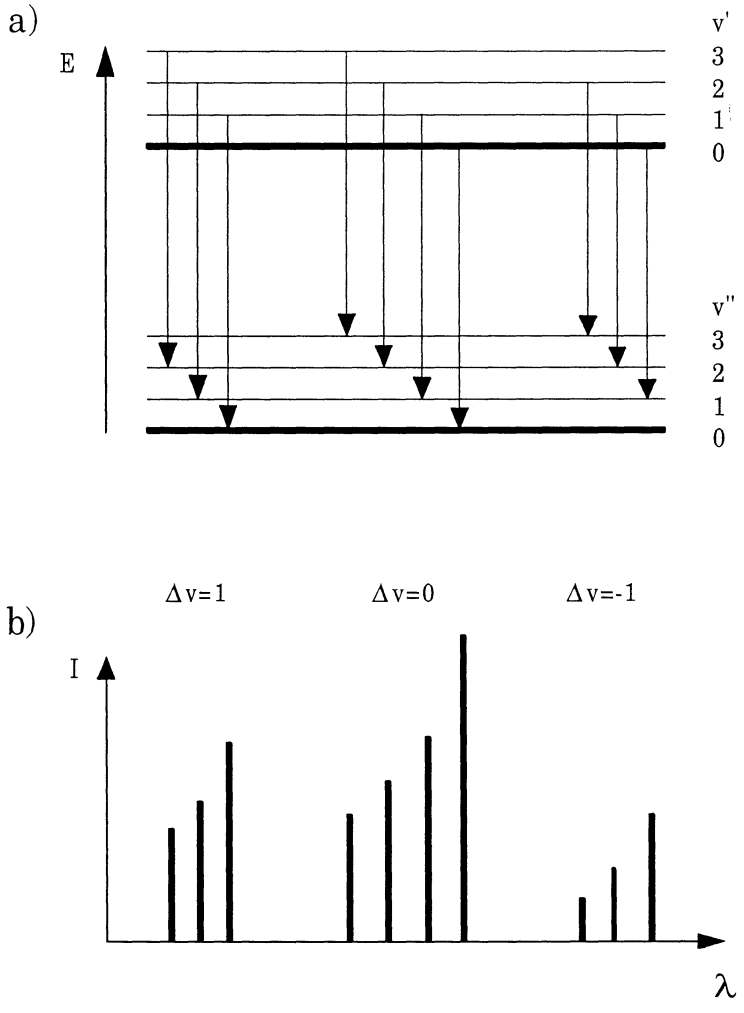

Fig. 3.1 a) *An energy level diagram of a molecule indicating vibrational splitting in two electronic states. Possible vibrational transitions between these two states are also shown.* b) *The spectral appearance of the emission for the marked transitions in* a. *Each line corresponds to the transition right above.*

The energy splitting caused by the vibrations is visualized in Fig. 3.1a. Emission lines corresponding to the indicated transitions are shown in Fig. 3.1b. In this figure the energy splitting is assumed to be greater in the upper level ($v'>v''$), why the bands are progressing to the violet - to shorter wavelengths. If the energy splitting is greater in the lower level, the bands are instead progressing to the red. (Compare the band systems of N_2 and AlO in Appendix A). As can be seen the lines will form *sequences* with equal Δv, these are also called diagonal groups. If, however, the vibrational splitting will be equal in the electronic levels ($v'=v''$), the transition energies will coincide and the sequences will consist of one line each.

3.3.2 Rotational energy

Vibrational lines in a spectrum will in turn be split up in finer lines. The reason for this is that a molecule rotates around its centre of gravity, thus yielding a rotational energy. The energy of a rotational state J measured from $J=0$, in cm^{-1}, is written as

$$F_v(J) = B_v J(J+1) - D_v J^2(J+1)^2 + \ldots, \tag{3.5}$$

where B_v and D_v are molecular constants being dependent on the vibrational quantum number, v, as well as the current electronic state. The selection rule for J is $\Delta J=0,\pm 1$[1]. We then get three different solutions to the transition energy, as this is a function of ΔJ, thus forming three series of lines - *branches*. As the distance between the lines will converge to zero, each branch will form a *band head.* This can be compared with the vibrational transitions, which appear with approximately constant spacing.

3.4 Evaluation of plasma parameters

As has been pointed out before, the unique properties of a plasma are determined by the electron gas and are thus dependent on the electron density and the kinetic temperature of the electrons. To characterize a plasma one must also know the temperatures of the atoms and molecules in a plasma, as these particles contribute to approximately all of the total mass of the system, and therefore will absorb most of the energy. In the case of a thermal equilibrium, all measured temperatures will be the same. This value will then correspond to what we normally mean when talking about a temperature. If the excitation is not thermal or does affect the thermal distribution, the methods mentioned below will give the *effective* temperatures.

1. If the projected component of the total angular momentum, Λ, is equal to zero in both states, then $\Delta J=0$ is forbidden. This is the case for a Σ^1 - Σ^1 transition [18].

3.4.1 Electron temperature

The intensity of an atomic line, at local thermal equilibrium (LTE) is given in Section 3.2.1. If a spectrum contains several lines from the same species and of the same ionization stage, it is possible to plot either $\ln I\lambda/g_i A_{ki}$ or $\ln I\lambda^3/g_k f_{ik}$ against the energy of the upper level, the excitation energy. The points should then fall on a line, with a slope equal to $-hc/kT_e$. Only relative line intensities is needed to do this Boltzmann plot. The electron temperature can of course also be found from the ratio of two lines

$$kT_e = \frac{E_2 - E_1}{\ln\{(I_1\lambda_1^3 g_2 f_2)/(I_2\lambda_2^3 g_1 f_1)\}}. \tag{3.6}$$

If LTE is not valid, no direct relation between line intensities and electron temperatures can be found and approximations for various equilibrium conditions have to be deducted.

One can also compare lines from the same element but in different ionization stages by using the Saha-equation (2.4) together with Eq. (3.1) [5].

3.4.2 Gas temperature

The gas temperature is related to the energy distribution among the heavier particles in a plasma. It can differ between different elements as well as it may be different than the electron temperature. The occurrence of molecular bands in a spectrum suggests a rather low temperature, insufficient to dissociate the molecules. The molecular lines may also be used for gas temperature determination. The band strength of a vibrational state, i.e. the sum of all line intensities emitted from an upper level divided by υ^4, is Boltzmann distributed in accordance to the vibrating energy of this state. We can therefore write [18]

$$\sum_{v''} \frac{I^{v',v''}}{\upsilon^4} = C\exp\left(-\frac{hcG(v')}{kT}\right), \tag{3.7}$$

where C is a constant. By plotting the logarithms of different band strengths versus the corresponding vibrational energy, a straight line should result, with a slope equal to $-hc/kT$.

It is often difficult to extract the gas temperature from the various vibrational transition emissions, as they frequently overlap. It may, therefore, turn out to be better to use the emission from various rotational levels instead. The intensity from a rotational line can be written as [18]

$$I = \frac{C\upsilon^4}{Q_r}(J'+J''+1)\exp\left(-B'\,J'\,(J'+1)\frac{hc}{kT}\right), \tag{3.8}$$

where C and Q_r are constants. The possible rotational quantum numbers J' and J'' of the different levels depend on the type of transition, i.e. the quantum numbers of the electronic states.

Line broadening of emitted light, in the case of a low electron density, is mostly due to the Doppler effect and thus depends on the velocities of the particles. A measurement of the halfwidth will thus reveal the kinetic temperature of the gas, as seen in Eq. (3.3).

3.4.3 Electron density

The electron density in a plasma is frequently obtained from measurements of the Stark broadening, comparing the recorded curve shape with theoretically calculated ones. Often the H_β-line of hydrogen is used for this purpose, since it is relatively easy to calculate and also has a relatively large broadening [15,19].

3.5 Other methods for plasma diagnostics

This chapter has so far been devoted to emission spectroscopy only, but a number of other methods are being used in plasma research. Some of these will be mentioned here, very briefly, together with informative references that treat these and other methods for plasma diagnostics. In Fig 3.2 is shown some methods for determination of the electron density.

Interferometry and holography
The electron density can be calculated from measurements of the refractive index. For this purpose, interferometric and holographic methods can be used. With holography, it is possible to obtain two-dimensional pictures of the density distribution [15].

Scattering of electromagnetic radiation
Externally produced electromagnetic radiation that is radiated on a plasma, will be scattered by the plasma particles - essentially by the electrons. The reflected radiation will thus yield detailed information about the distribution of the plasma particles [2,15,20].

Cyclotron radiation
Under the influence of a magnetic field, the electrons (and ions) will spiral around the field lines with characteristic frequencies. These are called electron cyclotron frequencies. The first harmonic usually appear in the microwave region. Studies of cyclotron radiation is nothing more than emission spectroscopy in the microwave region [2,15].

Probes
Various kinds of (electrical) probes are being used for plasma diagnostics. With those one can measure the plasma particle flux. The particle flux can yield both densities and tem-

peratures of the electrons and gas particles. A major drawback with these probes is that they must be inserted in the plasma, thereby they will change the conditions for the plasma being studied and the probes may also be damaged by the high temperature in the plasma [2,20].

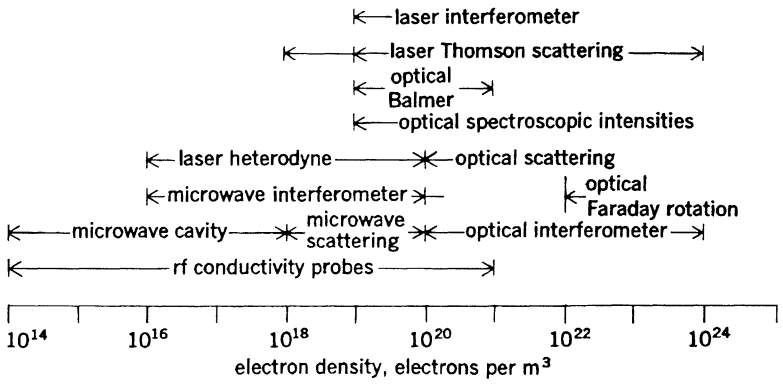

Fig. 3.2 *Methods and instruments for density measurements* [*13*].

4 Material and methods

4.1 Microwave plasma generator

A schematic drawing of the waveguide, which is connected to the plasma cavity is seen in Fig. 4.1. The microwaves are generated by a magnetron with a frequency of 2.45 GHz ±10 percent. The power of the incoming microwaves has in the experiments been adjusted within the range of 0.5 to 1.5 kW. To ignite a plasma, a copper wire conducts the current generated with a Tesla generator to the tip of the field concentrator. With this a spark is created. The spark causes the breakdown in the gas. For a brief theoretical description of the ignition, see Appendix E.

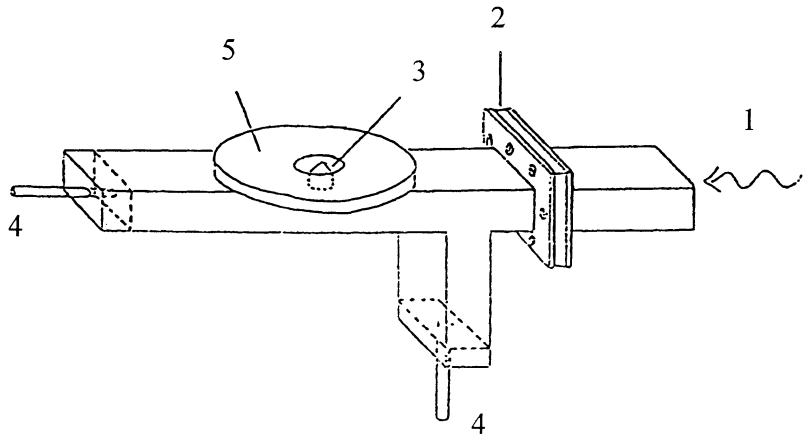

Fig. 4.1 *The waveguide of the microwave generator [1].* 1. *Microwave input.* 2. *Teflon window inserted to stop a plasma from reaching the magnetron.* 3. *Field concentrator.* 4. *Adjustable tuning shorts.* 5. *Platform on which the quartz tube was placed.*

The cavity consists of an 80 mm diameter tube of fused quartz surrounded by a copper mesh. The tube is placed on the platform and it is centred around the field concentrator. The copper mesh is connected to the waveguide with an aluminium ring. A similar ring is placed at the upper end of the quartz tube. A cylinder can be fitted in this ring. By displacing this cylinder, the height of the cavity can be adjusted. In the experiments carried out within the frame of this work, a cavity length of 167 mm, measured from the platform, was used.

Each of the used gases, except air, was filled from the bottom of the waveguide, close to the field concentrator. For the air experiments normal room air was used.

The plasma created was supposed to "float up" from the field concentrator and stay in the centre of the cavity away from the tube walls. This was very tricky to achieve. The tuning shorts had to be properly adjusted, especially the one at the top of the cylinder, (in order to not have a flame originating from the field concentrator). The plasma had a tendency to "float up" to the top of the cavity, where it could not be sustained. One way to stop this, apart from tuning, was to increase the microwave power. But at too high a power the plasma would start to go in the other direction - towards the magnetron. The plasma generation was furthermore dependent on the temperature of the waveguide and the cavity. The device had to be warm before the final adjustments could be done. The repeatability (during a day of experiments) in the plasma formation was good unless the setting was changed. In that case it was very difficult to get a plasma similar to what was produced previously.

4.2 Spectroscopic arrangement

The setup used in the experiments is shown in Fig. 4.2. The plasma was imaged with a lens on the end of an UV-grade optical fibre bundle. The fibre bundle guided the light to the spectrometer. The lens, having a diameter of 40 mm and a focal length equal to 50 mm, was made of fused silica. An optical filter, which blocked wavelengths below 5000 Å, was sometimes used in front of the fibre input, in order to suppress light below this wavelength before entering the spectrometer and thereby eliminating interference between this light, dispersed in higher orders, with light above this wavelength dispersed in the first order.

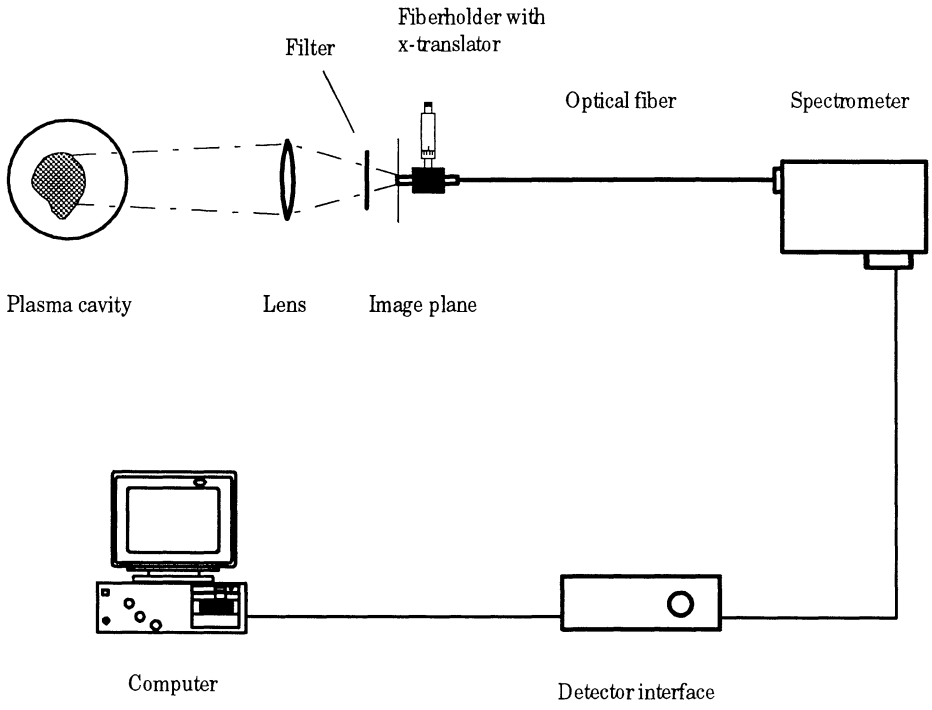

Fig. 4.2 *The spectroscopic arrangement during the measurements.*

The equipment used was supplied by EG&G Instruments. The spectrometer, Model 1235, is a Czerny-Turner design with a focal length of 275 mm. Two gratings where used with 150 g/mm and 300 g/mm and a dispersion of 0.6 and 0.3 nm/pixel, respectively. The dispersed light was recorded by a photodiode array detector, Model 1453A, controlled by the 1471A detector interface. The detector has a detection range of about 200 to 1100 nm. During the experiments the detector was operated at 25 °C. The drawback of a high dark current in the detector at room temperature was considered to be of minor importance. The data acquisition and subsequent analysis were performed with the OMA Vision-PDA software. The spectral sensitivity of the detector was calibrated using a calibrated blackbody radiator. The calibration with this lamp was not very reliable in the UV-region. A reference lamp for the UV-region was therefore ordered, but unfortunately not delivered in time to be used in the data analysis. Wavelength calibration was for the initial experiments accomplished using a low pressure mercury lamp, and later in the work using the identified atomic plasma lines.

4.3 Data acquisition

The data was collected with detector exposure times matching the strengths of the recorded signals. The exposure time was in most experiments set to 0.4-0.8 seconds. A measurement normally consisted of four to six consecutive recordings with a sample time being 0.41 s longer than the chosen exposure time. When studying the stability of a plasma, up to 15 consecutive data acquisitions, with a shorter exposure time, 0.06 s, was recorded immediately after each other (i.e. the sample time being equal to the exposure time).

Spectra were obtained from different parts of the plasma, using an x-translator to move the optical fibre end either horizontally or vertically. This was unfortunately not always possible because of the problems of creating similar plasmas. Due to the strong heat of the generated plasmas, these could not be driven continuously, without damaging the quartz tube (an exception from this is described in Section 5.4.2). This problem was increased by the fact that some plasmas was in direct contact with the tube. A new plasma had, therefore, to be generated for every measured point. Many of the measurements are therefore single shots, approximately from the centre of the imaged plasma. The range of the x-translator was not always sufficient when scanning through an image. The fibre holder then had to be moved, thereafter the measurements could continue from approximately the same location. A movement of the fibre holder has been marked in the plotted scans.

The setup had formerly been used with air and nitrogen [1], why these gases were first studied. Argon and helium were also used in the experiments, as they often are used in plasma research. Another reason for the choice of these gases was that they, in contrast to nitrogen and air, are atomic gases. An atomic gas was believed to yield different results.

4.4 Data analysis

The first step in the analysis was to **identify the emission lines in the recorded spectra** with the use of wavelength tables [5,21,22]. The molecular band systems were rather easily recognized, while the line radiation was harder to identify, because of the large amount of possible transitions for nearly all elements in the studied wavelength region. For some plasmas, **the intensity distribution** was measured. This was done by evaluating the peak intensity of an atomic line or a vibrational line in a band system.

The electron temperatures were obtained from Boltzmann plots for some of the observed atomic lines. To be able to do this, the difference in excitation energy between the lines included must be relatively large, the lines must not coincide with any of the other plasma lines and physical parameters for the elements studied must be available. The atomic data used in the calculations for the observed elements were taken from Refs. [23,24,25].

The vibrational temperatures were evaluated from the method mentioned in Section 3.5.2, using data from Refs. [18,26]. As the vibrational lines overlap, consistent results could only be obtained from the First positive system of nitrogen in nitrogen plasma and from the Green system of aluminium-oxide in air plasma.

No analysis of line broadening and rotational lines was performed, because of the requirement for a far better spectral resolution than was possible with the equipment used; about two orders of magnitude. It was, therefore, impossible to calculate the electron density and rotational temperatures or to obtain gas temperatures related to the velocity of the atoms and molecules via Doppler broadening.

The total intensity of a line is defined as

$$I = \int I(\lambda) d\lambda \,. \tag{4.1}$$

Thus one must take the area of a spectral line when deriving line ratios. This area was not easy to obtain with high accuracy. Instead, when analysing the lines of a band system, the line shapes were estimated from the spectrum. The intensity was then taken as the peak intensity, corrected for the background, times the full width at half maximum - FWHM, for each transition.

5 Results

5.1 Gas dependence of ignition

The generation of plasma in the setup utilized, proved to be very sensitive to the type of gas used as a medium in the cavity. While it was easy to create a plasma of air and nitrogen, ignition of helium and argon proved to be very difficult. With helium a small plasma was created at the tip of the field concentrator, causing it to melt. Ignition in the waveguide did also appear. In trying to ignite argon, visible plasma arcs from the field concentrator to the waveguide was seen. The argon plasma was also easily headed towards the magnetron. No measurements of pure argon and helium plasmas have, therefore, been performed.

The arcing of argon has also been observed by Kirsch *et al.* [27], who solved the problem by mixing the argon gas with water vapour. Other results show that mixing argon with another gas, even in very small amounts - e.g. 0.1% , can drastically change the temperature and density [6], as well as the size of the plasma in a microwave cavity [28]. Influenced by this the setup was changed to allow for mixing of two gases. It was then noticed that with helium present new kind of plasmas were created.

Table 5.1 *Measurements performed*

Plasma source	Electron temperature	Vibrational temperature	Intensity distribution	Ionization rate
Air	X	X		
Nitrogen		X	X	
He-air	X			
He-air-Ar	X		X	
He-N_2				X

The measurements in this work have been performed with the gases and gas mixtures listed in Table 5.1. In this table the properties that have been deducted from the various plasmas are also shown. The studied plasmas have all been maintained under a continuous gas flow. The intensity distribution for a nitrogen plasma was, however, measured both with and without a gas flow. These measurements show that a continuous supply of gas is required in order to maintain a stable plasma.

5.2 Air

Spectral analysis

A spectrum obtained from an air plasma is shown in Fig. 5.1. As can be seen, it is totally dominated by the OH-band at 3064 Å with small sidebands. Another significant signal for air is the NO-bands between 2100 and 2900 Å (see Fig. 5.2 and Appendix A). These bands are, however, much weaker. The occurrence of hydro-oxide or nitrogen-oxide bands in a spectrum from a plasma of any gas, indicates that air is present in the cavity.

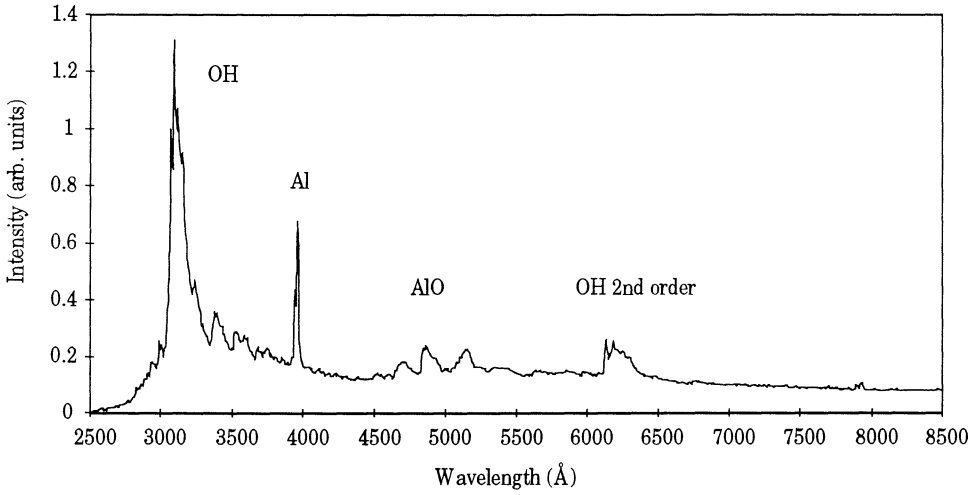

Fig. 5.1 *An air plasma. The spectrum is dominated by the 3064 Å band system of OH, also seen in the second order dispersion.*

In Fig. 5.2 is shown some atomic lines that could be seen at ignition and up to a few seconds after the ignition, for both air and nitrogen plasmas. The aluminium lines at 4000 Å were the most frequently appearing and yielded the highest intensity. They were most often accompanied by the AlO-band around 5000 Å.

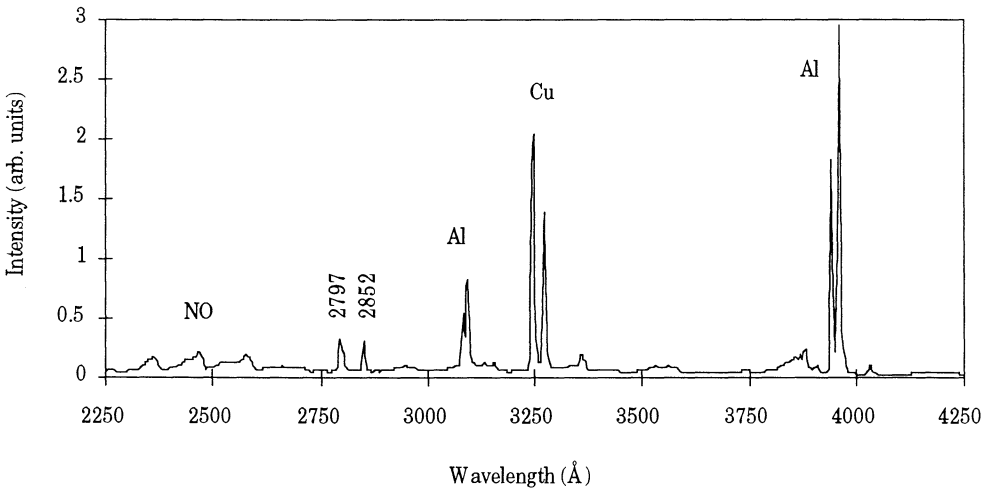

Fig. 5.2 *Atomic lines showing up at ignition. The recording is from a nitrogen plasma, but is valid for an air plasma as well. The two lines of shortest wavelength have not been identified.*

The atomic lines, that are seen in Figs. 5.2 and 5.3, are assumed to be from pollutants that are excited at the creation of the spark. They appeared very often during the experiments, if, however, somewhat randomized in appearance and intensity: sometimes totally dominating the spectrum, sometimes not seen. Some lines that were seen rather seldom, but always together with the other metal lines, have not been identified, see Fig. 5.3.

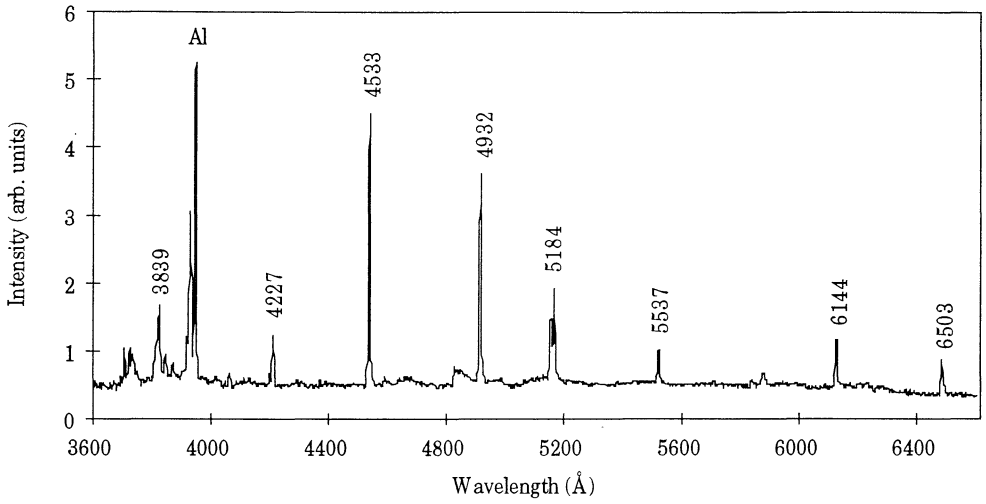

Fig. 5.3 *Unidentified lines seen at ignition of an air plasma.*

The electron temperature

The electron temperature was calculated from the slope of a Boltzmann plot of the four aluminium lines, see Fig. 5.4. The line intensities were obtained from recordings with negligible radiation from hydro-oxide, which otherwise coincide with the two lines of lower wavelength. The points in the plots are average values from three spectra. T_e was found to be 0.30 eV or 3500 K.

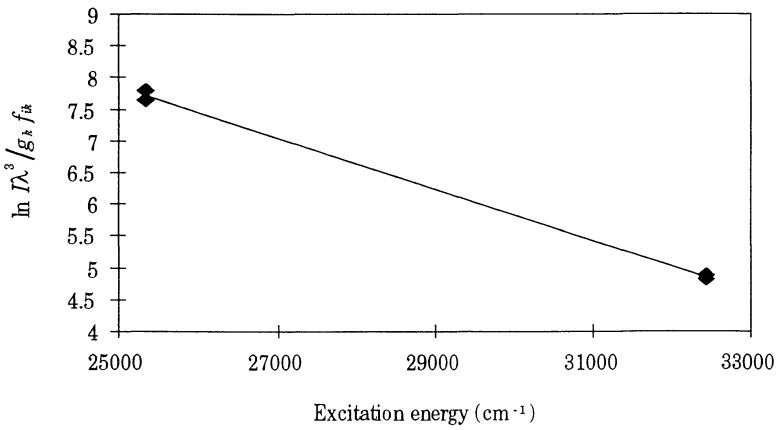

Fig. 5.4 *A Boltzmann plot for aluminium in a nitrogen plasma. The slope of the fitted line yields an electron temperature of 3500 K.*

The vibrational temperature

The vibrational temperature was determined from the observed band system of AlO. Fig. 5.5 shows the plot of $\ln\left(\sum_{v''}\frac{I^{v',v''}}{\upsilon^4}\right)$ versus $G(v')$. The slope of the least-square fit yields a vibrational temperature of 0.41 eV or 4800 K.

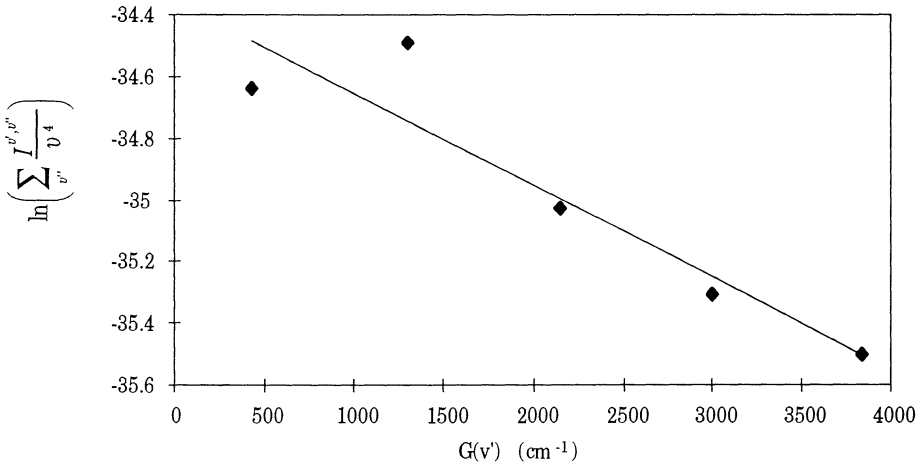

Fig. 5.5 *Plot for determination of the vibrational temperature of the Green system of AlO. The fit yields a vibrational gas temperature of 4800 K.*

5.3 Nitrogen

Intensity distribution

The first experiments with nitrogen plasma were performed by, during a short time immediately before the plasma ignition, filling the cavity with nitrogen gas. During the measurements there was then no supply of nitrogen gas. The plasma radiation characteristic for air, i.e. from OH and NO, was therefore rather obvious at the outer parts of the plasma and its intensity increased with time, until a pure air plasma had been created. The intensity distribution of this plasma radiation is seen in Fig. 5.6 a)-c), together with a schematic drawing of the plasma's location and appearance. As can be seen, the plasma was in contact with the tube wall. This was very common for nitrogen and air plasmas. The intensity distribution was recorded at three different heights, as indicated. The presence of air can be clearly seen throughout the entire plasma.

With a constant flow of gas, a homogenous nitrogen plasma, visually intense red, could be maintained. The intensity distribution of such a plasma is shown in Fig. 5.6 d), obtained as a scan from bottom to top. In this case radiation from NO and OH was only seen at the boundary of the plasma and the intensity was negligible. It must be emphasized that the location and distribution of a plasma were very dependent on the settings of the apparatus. Nitrogen plasmas located in the centre of the tube were obtained at some occasions. But after some changes in the instalment, this plasma location could not be recreated.

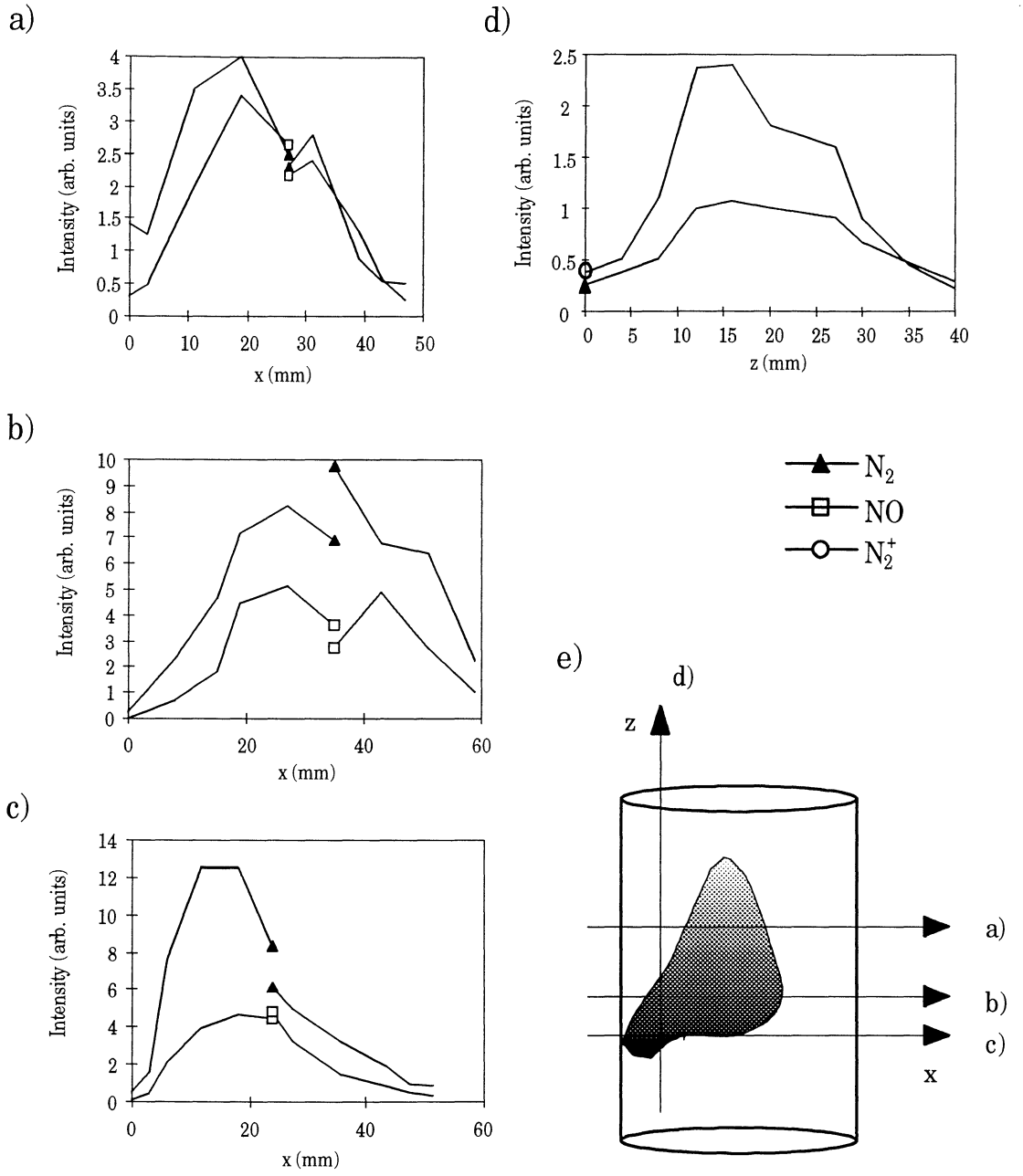

Fig. 5.6 *Relative intensity distributions of nitrogen plasma radiation. The performed scans are indicated in the schematic illustration of a plasma,* e. *In* a-c *are shown the results from plasmas with no nitrogen gas flow and in* d *with a constant flow of nitrogen gas. The break of a line mark a movement of the fibre holder, consult Section 4.3.*

Spectral analysis

As is shown in Fig. 5.7, a spectrum from nitrogen showed strong band heads in the red and the near-UV-region. The red band originates from the B→A transition in N_2, the so called First positive system. The other band system is the result of an overlap of two electronic transitions, the First negative system of N_2^+, a B→X transition, and the Second positive system of N_2 (C→B). The intensity of the radiation from the ionized molecules is much stronger. Consult Appendix A for more details of these band systems.

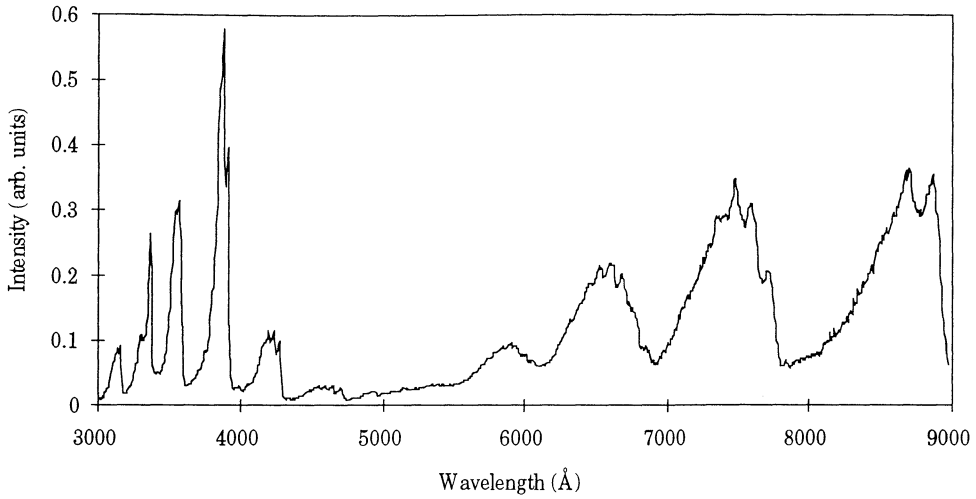

Fig. 5.7 *A nitrogen plasma showing radiation from neutral and ionized molecular nitrogen.*

The only atomic lines seen were from aluminium and copper, originating from the apparatus and taking part in the creation of the spark. Sequentially recorded spectra of a nitrogen plasma are presented in Fig. 5.8. As can be seen in the figure, the nitrogen plasma seems to be stable; the small intensity variations are probably due to changes in the gas density.

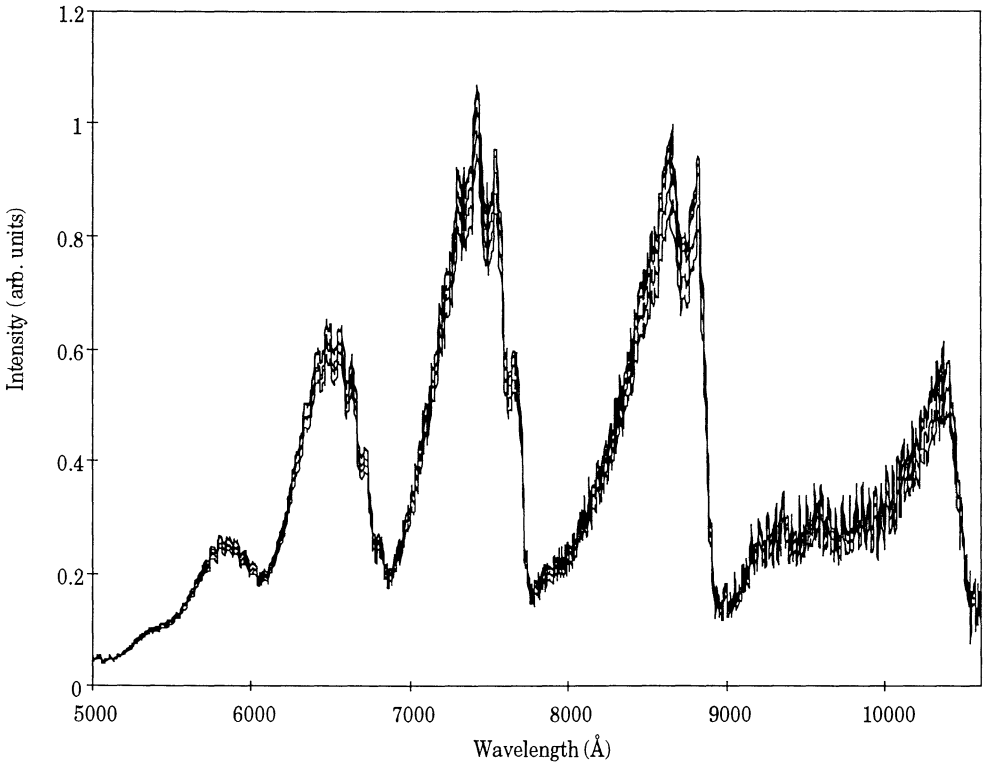

Fig. 5.8 *The First positive system of nitrogen in a nitrogen plasma. Five consecutive recordings of the same plasma show very small intensity variations and no difference in spectral shape. The exposure time was 0.06 s.*

The vibrational temperature

The vibrational temperature was calculated for the First positive system of nitrogen. The resulting plot is shown in Fig. 5.9. This gives an effective gas temperature of 5300 K or 0.46 eV.

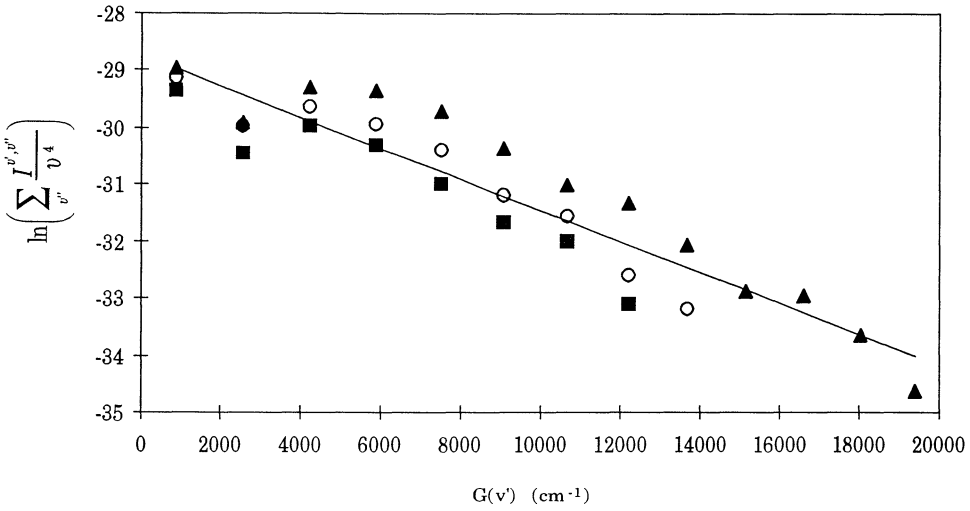

Fig. 5.9 *Plot for determination of the vibrational temperature of the First positive system of N_2. The temperature was evaluated to be 5300 K.*

5.4 Helium mixtures

Because of the instability of a pure helium plasma, a plasma of air or nitrogen was created before introducing helium. When adding helium to a gas the plasma decreased in size and got a more regular structure with a sharper boundary. It was also placed along the central line of the cavity, never in touch with the tube walls. The effect of adding helium was similar for a helium-air mixture with or without argon, but was somewhat different for the helium-nitrogen plasma, which will be discussed later. The volume fractions for the different gas mixtures have not been measured.

5.4.1 Helium - air

The addition of helium radically changed the behaviour of an air plasma. It first turned red-orange, and then slowly became white and transparent. During the first phase, the known bands of neutral and ionized nitrogen was seen. As the amount of molecular nitrogen decreased in a spectrum, atomic lines became visible. This progress, that can be seen in Fig. 5.10, is probably due to dissociation of the nitrogen molecules caused by higher energy absorption and, hence, a higher temperature. The line emission in the figure originates from neutral atoms of oxygen, nitrogen and hydrogen.

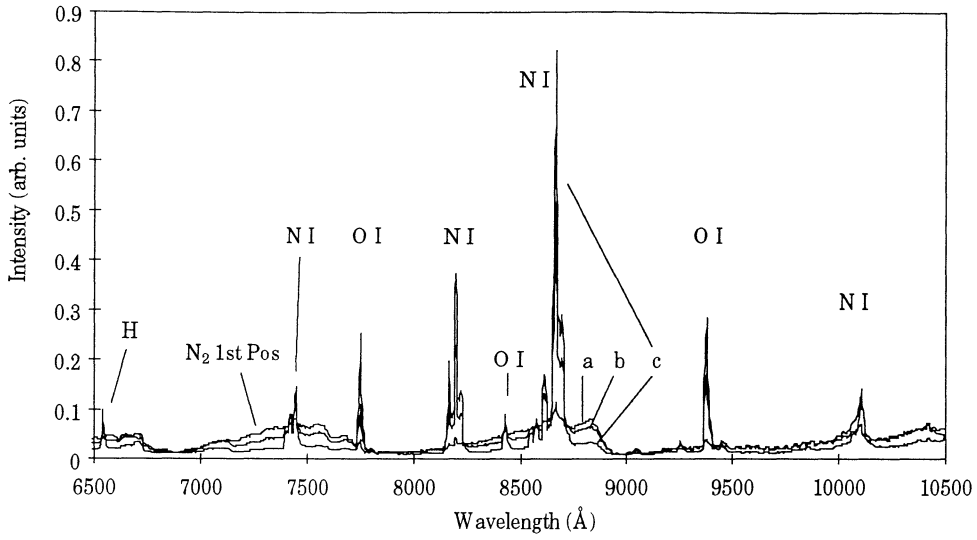

Fig. 5.10 *A helium-air plasma. The change of spectral components with time. a: 0-0.06 s, b: 0.24-0.30 s, c: 0.36-0.42 s. The amount of molecular nitrogen decreases, while atomic line emission becomes visible.*

The helium-air plasma was sinking in the cavity throughout this development, and it was finally ending up in the waveguide. Just before the helium-air plasma entered the waveguide, a much smaller, cigar-formed plasma, that was located some millimetres above the platform could be created. This transformation appeared rather randomly during the change of the gas flows, the reason therefore being unknown. Once it had occurred, this plasma showed to be extremely stable and fixed. The cigar plasma could be maintained for several tens of seconds without causing the copper mesh around the quartz tube to glow.

The helium-air plasmas were sensitive to the rate of the helium flow; if this was too high the plasma headed towards the magnetron.

Spectral analysis

As can be seen in Fig 5.10, spectral recordings from a helium-air plasma showed a number of atomic lines from different elements in the visible and near infrared regions. In the figure is not seen any lines of helium. Line emission from helium did, however, appear, but, for some reason, not on every recording. The shortest line emission observed in these experiments, was the H_γ-line at 4340 Å. In the near-UV the observed radiation originated from molecules, such as the line-like NH-band at 3358 Å, as seen in Fig. 5.11.

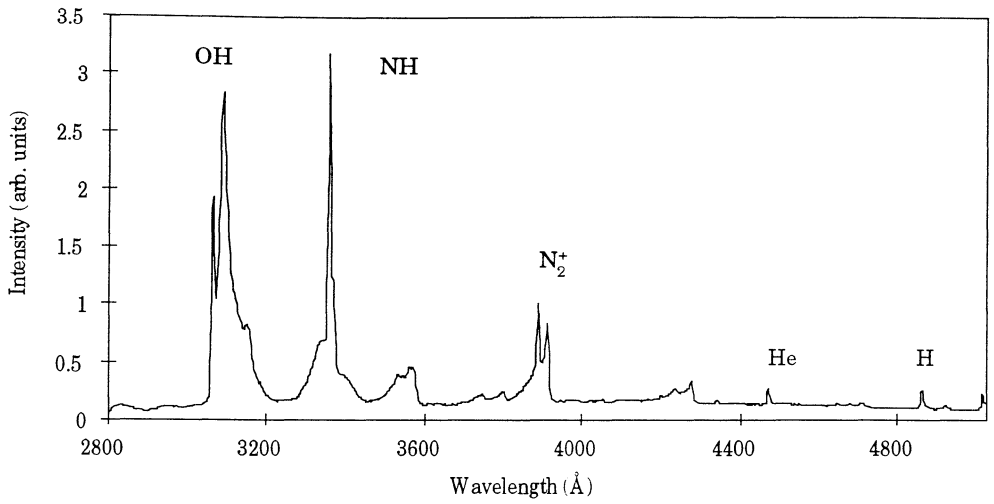

Fig. 5.11 *A helium-air plasma. Only molecular radiation can be seen below the very weak H_γ-line at 4340 Å.*

5.4.2 Helium - air - argon

Spectral analysis

Spectra obtained from a helium-air-argon plasma were identical to spectra taken from a helium-air plasma, except for a number of argon lines. These occurred between 7000 and 10000 Å, as shown in Fig. 5.12.

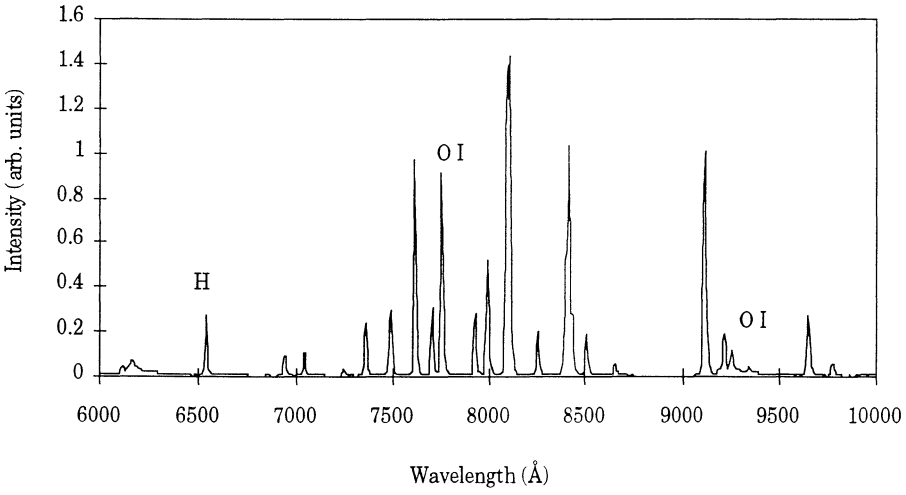

Fig. 5.12 *Line emission from a helium-air-argon plasma. All non-marked lines are from neutral argon.*

The intensity distribution

If argon was added to a helium-air plasma, the plasma was only affected in one way: if the argon flow was too high, the plasma went down in the waveguide. The cigar plasma did appear also during these measurements. The intensity distributions for various observed plasma lines of this stable plasma are shown in Fig. 5.13. It can be seen that the plasma has a sharper boundary closer to the field concentrator and the gas flow. The tail on the upper side has been seen from other plasmas as well throughout the experiments (see e.g. Fig. 5.6). Each intensity scan on the cigar plasma was performed on the very same plasma, maintained during the scanning.

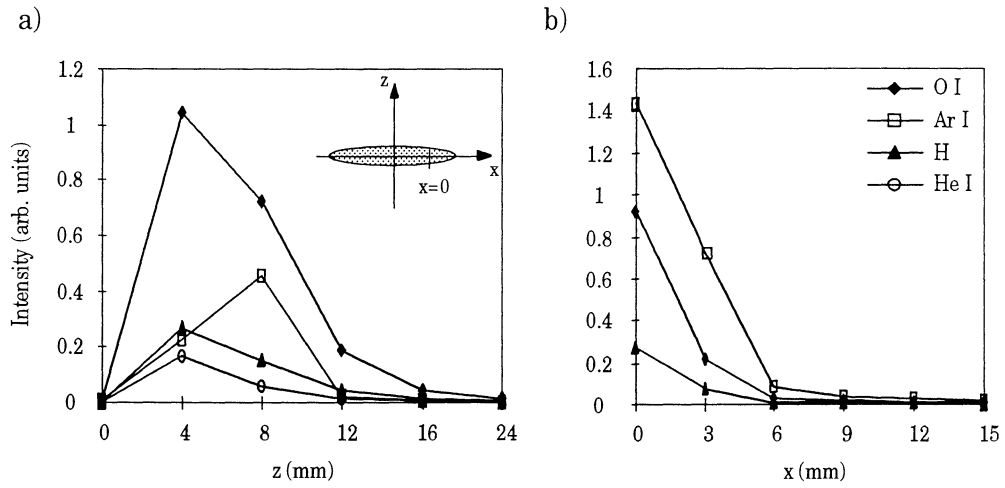

Fig. 5.13 *Relative intensity distribution of the cigar-formed helium-air-argon plasma.* a) *shows the vertical distribution, going from bottom to top, and* b) *shows the horizontal distribution when scanning through the boundary of the plasma. Do note the absence of helium in the horizontal scan.*

The electron temperature

For the helium-air and helium-air-argon plasmas Boltzmann plots have been calculated for all elements observed. These plots are shown in Fig. 5.14. The points in the plots do not always fall along a line. This is in agreement with the assumption that LTE does not hold. For this reason not all transitions were included in the least-square fits. For Ar I and O I has no line at all been calculated.

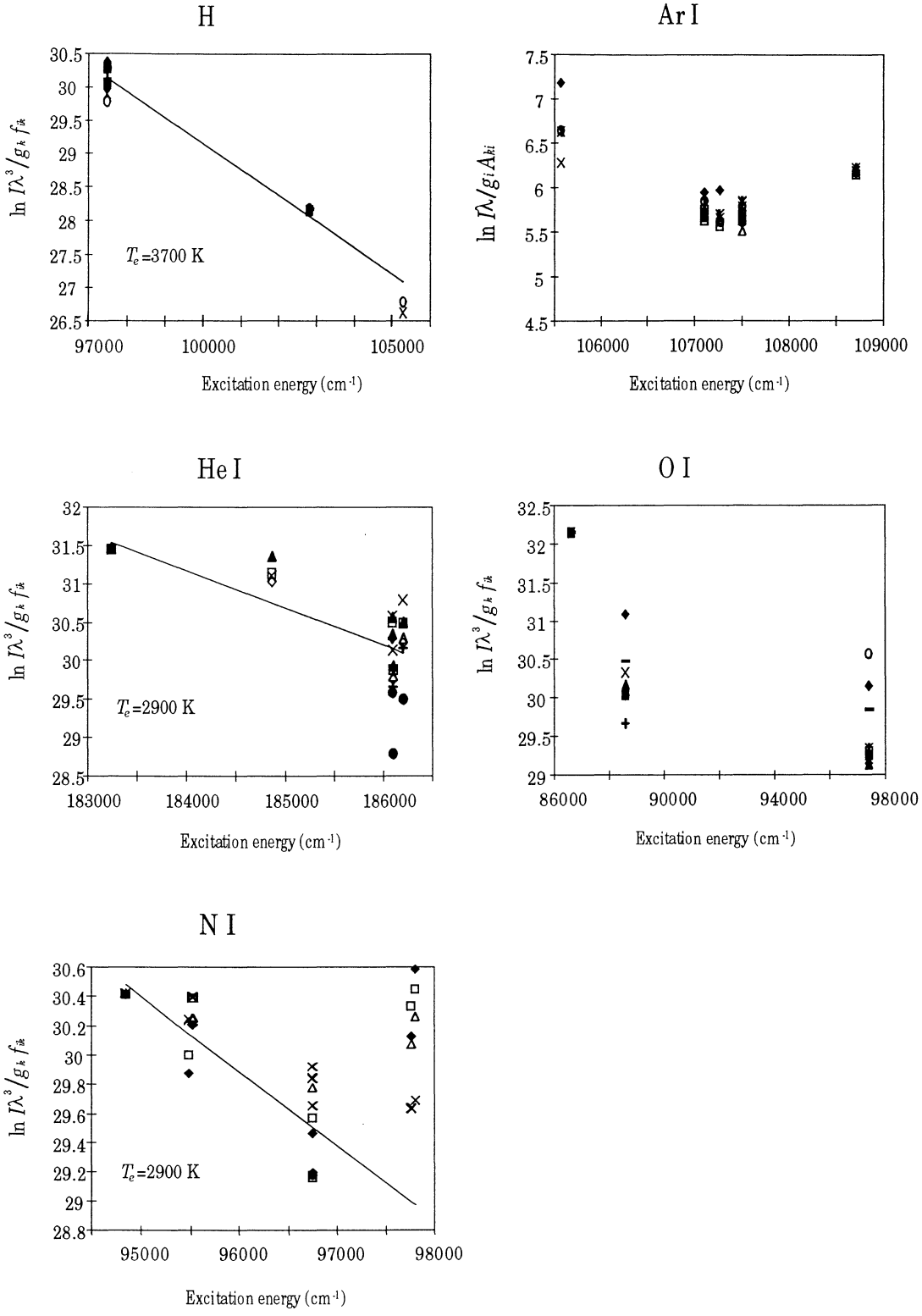

Fig. 5.14 *Boltzmann plots for H, He I, N I, O I and Ar I. Different markers represent different recordings, which have been made for helium-air and helium-air-argon plasmas. Each plot have been standardized to one transition that was seen in every recording. For N I was the two transitions of highest excitation energy omitted in the fit of the line. No lines for Ar I and O I are presented, as the slopes of these have an unacceptable variation. The values are, however, in the same order as the results of the other elements.*

The electron temperatures obtained for each species are given in Table 5.2. There is also tabulated, for every element, the highest energy levels from which visible deexcitations have been seen and the lowest wavelength observed. The value for aluminium was obtained from an air plasma, consult Section 5.2.

Table 5.2 *Electron temperatures with highest energy levels seen excited and lowest wavelength observed.*

Element	T (K)	T (eV)	E (eV)	λ (Å)
H	3700	0.32	13.06	4340
He I	2900	0.25	23.74	4471
N I	2900	0.25	12.98	7423
Al I	3500	0.30	4.02	3082
Ar I			13.48	6965
O I			12.08	7773
Cu I			3.82	3247

5.4.2 Helium - nitrogen

This plasma had, in contrast to the mixtures of helium with air and argon, no tendency of going down in the waveguide; it was not influenced when increasing the gas flow of nitrogen. The plasma remained firmly placed some centimetres up in the tube.

Spectral analysis

The spectra recorded from this plasma were different from the ones obtained from the helium-air plasma. Normally, the familiar band systems of molecular nitrogen were seen. But at some occasions no radiation from ionized nitrogen did occur, the Second positive system of nitrogen thereby being clearly resolved. No atomic lines were seen with this mixture.

The ionization rate

It was noticed that the rate of ionization of molecular nitrogen was increased when introducing helium to a nitrogen plasma. Calculations show that the intensity ratio $I_{tot}(N_2^+,1stNeg)/I_{tot}(N_2,1stPos)$, was increased from 0.14 to 1.1, i.e. about eight times. The total intensities of the bands were evaluated by using the area-calculation facilities provided by the OMA vision-PDA software. Some corrections to these calculated values were, however, made, as described in Appendix D.

No vibrational temperatures could be obtained from the helium-nitrogen plasma, as the vibrational transitions where strongly overlapped and the line profiles therefore impossible to estimate.

6 Discussion and conclusions

6.1 Summary and discussion

6.1.1 Spectral analysis

Plasmas of air or nitrogen showed molecular radiation only from the partitioning gases. The energy absorbed was not sufficient to break the molecular bonds. Line emission was seen from pollutants in the cavity (as aluminium from the field concentrator and copper from the wire to the Tesla generator), that were excited by the plasma at the ignition. Their excitation energies lie clearly below the dissociation energies of oxygen and nitrogen, which are 5.1 and 9.8 eV, respectively.

Atomic line emissions from the gases used for the plasma production were only seen if helium was added. Electronic transitions were observed from all elements, but for neutral atoms only. The collision frequency was probably not high enough to excite the ions before they recombined. The kinetic energy of the electrons may, also, have been insufficient to excite the ions in the plasma to levels with visible deexcitations. The observed excitation energies for all elements, except for helium, were about 12 to 13 eV. For helium the energies were about 24 eV. The reason for this discrepancy has not yet been fully understood. An interesting fact was that on some recordings no radiation from helium could be seen. The shortest wavelength observed, from any of the gases that has been used as plasma source, was the H_γ-line of hydrogen at 4340 Å. Most of the line radiation did, however, occur around 8000 Å. From the pollutants two lines around 2800 Å were often observed.

The results are affected by the fact that the cavity was not sealed and that air was always present during the measurements. Radicals were created in the plasma and had a higher abundance at the plasma boundary. This is rather natural as air must be present for these to exist. Radicals that have been observed are: O I, OH, NO and NH.

6.1.2 Intensity distribution

The intensity distributions, as well as size and location, of the plasmas were very dependent on the settings of the plasma generator and the used gas. In all distributions measured, it was noticed that the plasmas had a sharper intensity boundary closer to the field concentrator and the gas flow. At the top, the intensity decreased more slowly, the plasma having a tail, which for pure air or nitrogen plasmas could almost reach to the top of the cavity. With helium mixtures the visual appearance of the plasmas was more homogenous and smooth and the plasmas were located along the line of centre in the cylindrical tube. The difference in appearance, in comparison with the air and nitrogen plasmas, was remarkable.

6.1.3 Temperature measurements and equilibrium

When trying to extract the plasma temperatures from the emitted light, different theoretical models can be utilized, dependent on the type of equilibrium characterizing the plasma. Some models have been discussed above. The approximate evaluations of temperatures performed in this paper have assumed local thermal equilibrium. For LTE to hold, the system temperature should be about 10000 K (0.9 eV). This is, however, not the case here. The limited line radiation observed, gives more an impression of a corona-like state of the plasmas. No usable method of temperature determination for this state of equilibrium has been found.

Another great problem with the temperature determination is the accuracy of the calculated values. Estimations of the intensities of vibrational transitions in a band system were very difficult to perform due to considerable line overlapping. That is the reason why only two of the observed band system have been used. Tabulated oscillator strengths and transition probabilities are often not correct and should be used with care. In Ref. [21], the error of the values for hydrogen and helium is estimated to about 1-3%. For oxygen and nitrogen Wiese *et al.* estimates the error to be about 25%. In some of the plots, points for some transitions clearly fall outside an approximate line. All transitions have not been used in the least-square fit for nitrogen, and for oxygen and argon no electron temperatures are presented. The choice of doing this may be discussed, but for these plots no unique line does exist. It should also be mentioned, that a visually small change of the slope of any of the calculated lines in the plots, would affect the resulting temperature significantly.

The most line-like Boltzmann plots are those for hydrogen, helium and aluminium. The errors of these values have been estimated, from the variations in the plots, to be in the order of 0.05 eV (600 K). This has been done with the assumption that the atomic data have small errors. The accuracy of the vibrational temperatures in air and nitrogen plasmas are more difficult to estimate, since the intensities are tricky to measure. The errors of the vibrational gas temperatures should then be greater than for the electron temperatures; probably with at least a factor of two. The presence of as many vibrational transitions indicates that the vibrational temperatures are high. When the temperature in a plasma increases, the thermal energy becomes greater and electrons can be excited to even higher vibrational levels, wherefore more transitions can be seen, see Fig. 3.1. That the vibrational temperatures differ from the electron temperatures is not surprising, as thermal equilibrium is assumed not to hold. Also, the vibrational temperatures are measured from other kinds of plasmas than most of the electron temperatures.

The question of the value of the effective temperature in the studied plasmas then remains. Since thermal equilibrium is assumed not to hold, no single well-defined temperature does exist. It is not possible to describe the energy content of the plasmas with one temperature. In order to describe the system, different temperatures, such as the calculated electron and vibrational temperatures, have to be used. In practical applications it may, however, be interesting to know the effect the generated plasmas will have on a material, in terms of a temperature. Some conclusions can then be drawn from the obtained results and from some material constants. As the plasmas cause the copper mesh to glow (this was not observed for the so called cigar plasma), the temperature at the outer side of the quartz tube should reach values in the order of the melting point of copper, which is 1356 K. The tube itself can stand temperatures of about 1500 K without getting damaged; and no

damage to the tube was observed. The temperature could for these reasons be guessed to be 1000 to 1500 K at the boundary, and probably higher in the centre of the plasmas. As the measured values do not significantly differ from this guess, a more accurate value of the effective temperature in the plasmas can not be drawn from this study.

6.14 The ionization rate

The only ion observed from all spectral recordings made for this study is N_2^+, ionized molecular nitrogen. The absolute rate of ionization has not been determined. This would require the knowledge of all transition probabilities between the different states involved. When helium was added to a nitrogen plasma, it was noticed that the intensity ratio between the First negative system of N_2^+ and the First positive system of N_2 was increased with approximately a factor of 8. This suggests that the rate of ionization increases when adding helium. Exactly how much the increase was, is, however, difficult to measure. The presence of helium might cause that a higher amount of the nitrogen molecules were excited to higher states, yielding a lower emission intensity from the First positive system and a higher intensity from the Second positive system. The, normally, much lower intensity of the Second positive system is in these calculations added to the intensity of the ionized nitrogen, due to overlapping.

6.2 Conclusions

The aim of this work has been to study the properties of plasmas generated in a microwave cavity at atmospheric pressure. Emission spectroscopy has been used to measure the kinetic temperatures of the plasma particles and their relative distribution. As plasma sources have been used gases of air, nitrogen and mixtures of helium with air, argon and nitrogen.

It has been found, that cold plasmas were created in the cavity using the gases and mixtures of gases studied. The studies yield that the maintained plasmas were stable and thus in some state of equilibrium. The type and conditions of the equilibrium have not been fully determined, but a coronal state of the plasmas is suggested. The time-scale of the observations in this study is, however, in tenths of seconds. This is a very long time in comparison to the lifetimes of the observed excited states. Non-equilibrium conditions might occur shortly after the ignition. The temperatures determined in this work are not very accurate and should be used with caution.

No plasmas of absolutely pure gases could be created with this device, as air always, to some extent, was present in the cavity. The air content lead to the presence of radicals in the plasmas (O I, NO, NH, OH). The very presence of air can strongly affect the plasma properties, why other results may have been obtained if the cavity would have been sealed off and free from air. It would, also, have been interesting to test hydrogen in the generator, especially after the results with helium. To avoid an explosive reaction between hydrogen and oxygen, this should not be done as long as it is not possible to have the cavity completely free from air.

The pollutants introduced at ignition, may also affect the plasmas. However, as their amount decreased to zero within a few seconds and no spectral changes could be noticed during the decrease, their influence are considered to be small. The presence of pollutants in a plasma can also be of advantage. A properly chosen element can be added to a plasma in order to study the properties of the plasma, and perhaps also the influence the plasma has on the element. In this work aluminium has been used to calculate the electron temperature in plasmas unable to yield line emission from the plasma source elements.

A major problem throughout the experiments, has been the reproducibility in creating and maintaining plasmas. The sensitivity to the tuning of the generator and the lack of control of the plasma generation have limited the possibilities for systematic measurements. My suggestion is, that a better understanding of the function of the microwave generator and the coupling of the microwave power to the plasma will be required, if further studies are to be performed. Especially if future applications are to be examined, the plasma generation must be better controlled.

Acknowledgements

First of all, I would like to thank my supervisors Ph.D. Stefan Andersson-Engels and Ingmar Andréason, who have guided me through this project.

I would also like to thank those of their colleges, who have helped me with various kinds of problems during my work.

References

1. E. Eyoma, *Investigation of the Surface Treating Properties of a Microwave Induced Plasma at Atmospheric Pressure*, Lund University, Department of Applied Electronics, Lund (1994).

2. I.H. Hutchinson, *Principles of plasma diagnostics*, Cambridge University Press, New York (1987).

3. P.K. Carroll and E.T. Kennedy, *Laser-Produced Plasmas*, Contemp. Phys. **22**, 61-96 (1981).

4. A. von Engel, *Ionized gases*, Oxford University Press, London (1965).

5. H.R. Griem, *Plasma Spectroscopy*, McGraw-Hill, New York (1964).

6. H. Haken and H.C. Wolf, *Atomic and Quantum Physics*, Springer-Verlag, Berlin (1987).

7. M.H. Gordon and C.H. Kruger, *Nonequilibrium effects of diluent addition in a recombining argon plasma*, Phys. Fluids B **5**, 1014-1023 (1993).

8. K.-P. Nick, J. Richter and V. Helbig, *Non-LTE diagnostic of an argon plasma*, J. Quant. Spectrosc. Radiat. Transfer **32**, 1-8 (1984).

9. P.W.J.M. Boumans, F.J. deBoer and J.W. de Ruiter, *A stabilized r.f. argon-plasma torch for emission spectroscopy*, Philips tech. Rev. **33**, 50-59 (1973).

10. H. Herman, *The Plasma State and its Industrial Utility*, In: *1st Plasma-Technik-Symposium. I*, (1988).

11. G. Kristensson, *Elektromagnetisk vågutbredning*, Lund University, Lund (1994) (In swedish).

12. P.A. Sturrock, *Plasma physics*, Cambridge University Press, Cambridge (1994).

13. *McGraw-Hill encyclopedia of science and technology*, McGraw-Hill, New York (1987).

14. E.T. Kennedy, *Plasmas and Intense Laser Light*, Contemp. Phys. **25**, 31-58 (1984).

15. V.E. Golant, *Methods of diagnostics based on the interaction of electromagnetic radiation with a plasma*, In: *Basic Plasma Physics II*, A.A. Galeev and R.N. Sudan (eds.), North-Holland, Amsterdam (1984).

16. C.H. Corliss and W.R. Bozman, *Experimental Transiton Probabilities for Spectral Lines of Seventy Elements*, NBSM 53, US Government Printing Office, Washington (1962).

17. H.R. Griem, *Radiation processes in plasmas*, In: *Basic Plasma Physics I*, A.A. Galeev and R.N. Sudan (eds.), North-Holland, Amsterdam (1983).

18. G. Herzberg, *Molecular Spectra and Molecular Structure. Vol 1. Spectra of Diatomic Molecules*, Van-Nostrand, New York (1950).

19. W. Lochte-Holtgreven, *Evaluation of plasma parameters*, In: *Plasma diagnostics*, W. Lochte-Holtgreven (ed.), North-Holland, Amsterdam (1968).

20. W. Lochte-Holtgreven (ed.), *Plasma diagnostics*, North-Holland, Amsterdam (1968).

21. R.W.B. Pearse and A.G. Gaydon, *The Identification of Molecular Spectra*, Chapman and Hall, London (1976).

22. A.R. Striganov and N.S. Sventitski, *Tables of spectral lines of neutral and ionized atoms*, IFI Plenum, New York (1968).

23. W.L. Wiese, M.W. Smith and B.M. Glennon, *Atomic Transiton Probabilities. Hydrogen through Neon*, NSRDS-NBS 4, US Government Printing Office, Washington (1966).

24. R.A. Nodwell, J. Meyer and T. Jacobson, *Radiative transition probabilities between the $3p^5 4p$ and $3p^5 4s$ configurations of neutral argon*, J. Quant. Spectrosc. Radiat. Transfer **10**, 335-340 (1970).

25. D.C. Morton, *Atomic data for resonance absorption lines. I. Wavelengths longward of the Lyman limit*, Astrophys. J. Suppl. Ser. **77**, 119-202 (1991).

26. K.P. Huber and G. Herzberg, *Molecular Spectra and Molecular Structure. Vol 4. Constants of diatomic molecules*, Van-Nostrand, New York (1979).

27. B. Kirsch, S. Hanamura and J.D. Winefordner, *Diagnostical measurements in a single electrode, atmospheric pressure, microwave plasma*, Spectrochim. Acta **39B**, 955-963 (1984).

28. J. Hubert, M. Moisan and A. Ricard, *A new microwave plasma at atmospheric pressure*, Spectrochim. Acta **33B**, 1-10 (1978).

29. M. Moisan and J. Pelletier (eds.), *Microwave Excited Plasmas*, Elsevier, Amsterdam (1992).

30. S. Bashkin and J.O. Stoner, Jr., *Atomic Energy Levels and Grotrian Diagrams. Volume I*, North-Holland, Amsterdam (1975).

31. S. Bashkin and J.O. Stoner, Jr., *Atomic Energy Levels and Grotrian Diagrams. Volume II*, North-Holland, Amsterdam (1978).

Appendices

A Observed band systems

In this appendix transitions from the observed band systems are listed. The data are taken from Ref. [21]. Variables and quantum numbers are defined and explained in Ref. [18].

AlO Green system, $B^2\Sigma^+ - X^2\Sigma^+$

Degraded to the red.

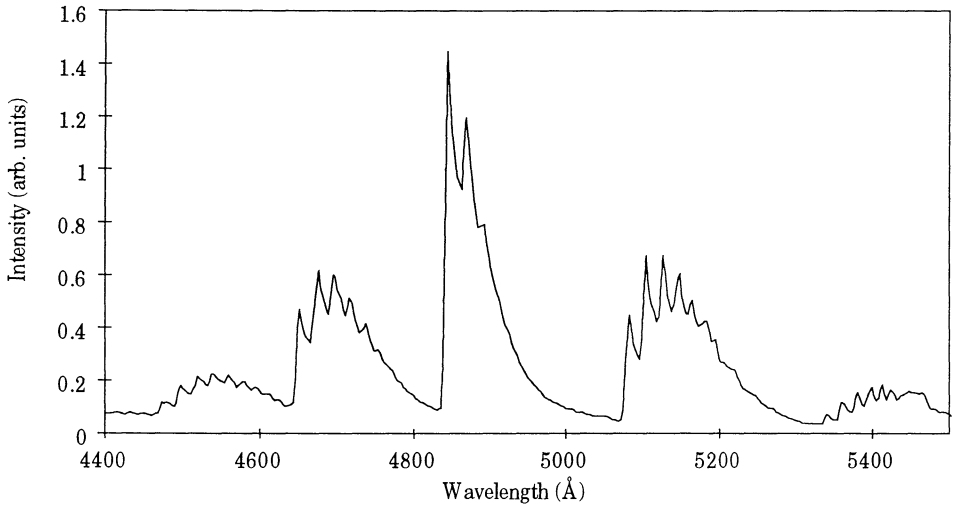

Fig. A.1 *The Green system of AlO obtained from an air plasma.*

Wavelength	v'	v''	Wavelength	v'	v''
5357.8	1	3	4671.9	2	1
5337.0	0	2	4648.1	1	0
5102.0	1	2	4493.8	3	1
5079.4	0	1	4470.4	2	0
4866.2	1	1			
4842.2	0	0			

N_2 First positive system, $B^3\Pi_g - A^3\Sigma_u^+$

Degraded to the violet

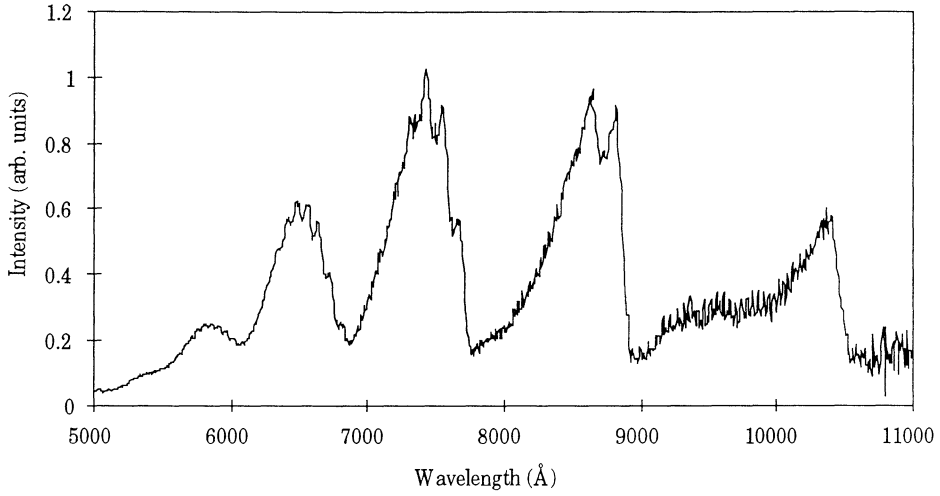

Fig. A.2 *The First positive system of nitrogen obtained from a nitrogen plasma.*

Wavelength	v'	v''	Wavelength	v'	v''
10510.0	0	0	6875.0	3	0
9942.0	2	2	6788.6	4	1
9682.1	3	3	6704.8	5	2
9436.4	4	4	6623.6	6	3
9203.9	5	5	6544.8	7	4
8912.4	1	0	6185.2	4	0
8722.3	2	1	6127.4	5	1
8541.8	3	2	6069.7	6	2
8369.2	4	3	6013.6	7	3
8204.8	5	4	5959.0	8	4
7753.2	2	0	5632.7	5	0
7626.2	3	1			
7503.9	4	2			
7386.6	5	3			
7273.3	6	4			

N_2 Second positive system, $C^3\Pi_u - B^3\Pi_g$

Degraded to the violet.

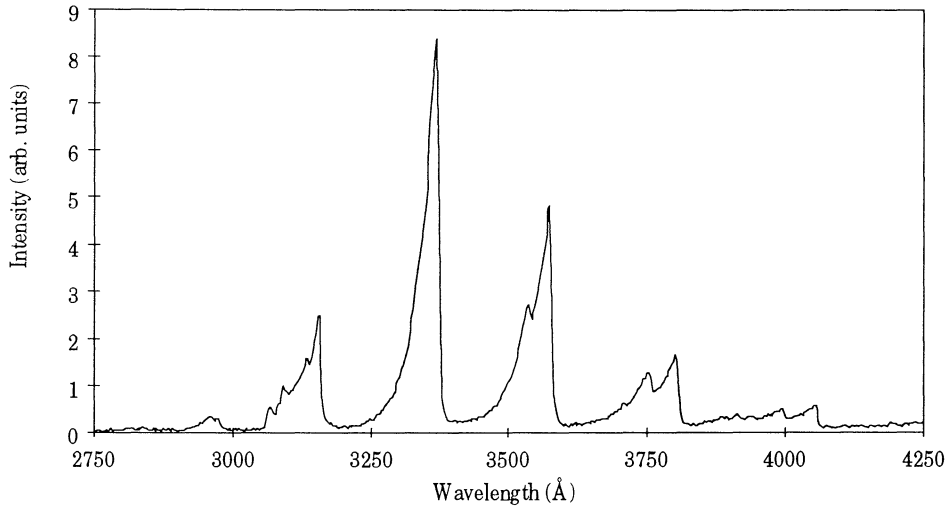

Fig. A.3 *The second positive system of nitrogen obtained from a helium-nitrogen plasma. The plot has not been intensity calibrated, which has no qualitative influence on its look*

Wavelength	v'	v''	Wavelength	v'	v''
4059.4	0	3	3371.3	0	0
3998.4	1	4	3339	1	1
3943.0	2	5	3309	2	2
3804.9	0	2	3159.3	1	0
3755.4	1	3	3136.0	2	1
3710.5	2	4	3116.7	3	2
3576.9	0	1	2976.8	2	0
3536.7	1	2	2962.0	3	1
3500.5	2	3	2953.2	4	2

N_2^+ First negative system, $B^2\Sigma_u^+ - X^2\Sigma_g^+$

Degraded to the violet.

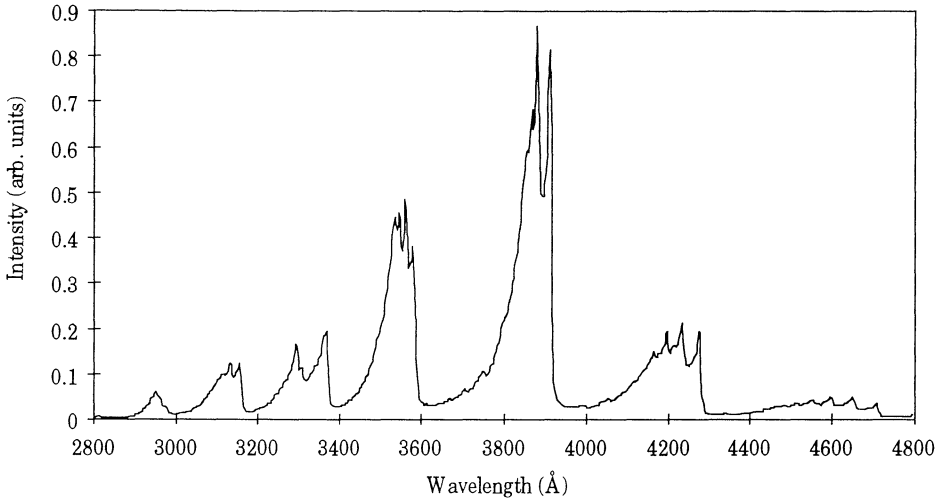

Fig. A.4 *The First negative system of singly ionized nitrogen obtained from a nitrogen plasma.*

Wavelength	v'	v''	Wavelength	v'	v''
4709.2	0	2	3582.1	1	0
4651.8	1	3	3563.9	2	1
4599.7	2	4	3548.9	3	2
4278.1	0	1	3308.0	2	0
4236.5	1	2	3298.7	3	1
4199.1	2	3	3293.4	4	2
3914.4	0	0			
3884.3	1	1			
3857.9	2	2			

NH 3360 Å system, $A^3\Pi - X^3\Sigma^-$

Non-degraded.

Wavelength	Branch	v'	v''
3370	Q	1	1
3360.1	Q	0	0
3317.0	R	1	1
3302.5	R	0	0

NO γ system (Nitrogen third positive), $A^2\Sigma^+ - X^2\Pi$

Degraded to the violet. Double headed.

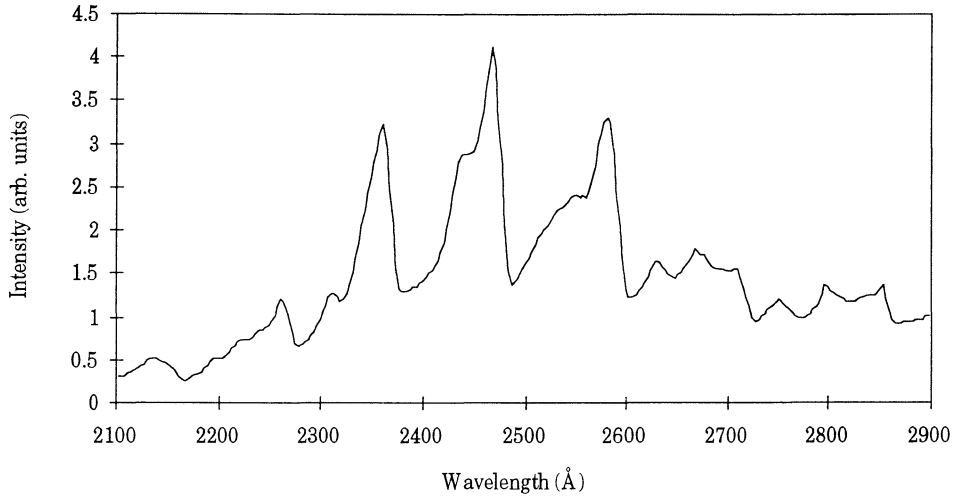

Fig. A.5 *The γ system of NO obtained from a nitrogen plasma. The plot has not been intensity calibrated.*

Wavelength	v'	v''	Wavelength	v'	v''
2859.5	0	5	2478.7	0	2
2849.8			2471.1		
2722.2	0	4	2370.2	0	1
2713.2			2363.3		
2595.7	0	3	2269.4	0	0
2587.5			2262.8		
			2154.9	1	0
			2149.1		

OH 3064 Å system, $A^2\Sigma^+ - X^2\Pi$

Degraded to the red.

Wavelength	Branch	v'	v''
3063.6	R	0	0
3067.2	R	0	0
3078	Q	0	0
3089	Q	0	0

B Observed spectral lines

Most of the observed emission lines are listed here with their respective excitation energy. Data are taken from Refs. [16,22,23]. Conversions from inverse centimetres to electron volts can be done by the relation: 1 cm^{-1} = 1.23992·10^{-4} eV. The tabulated values for argon were originally in eV. m indicates multiple lines.

Element	Wavelength (Å)	E_i (cm^{-1})
H	4340.46	105292
H	4861.32	102824
H	6562.8	97492
He I	4471.5	191445
He I	5015.68	186210
He I	5875.7	186102
He I	6678.15	186105
He I	7065.3 m	183237
He I	7281.35	184865
N I	7423.64	96752
N I	7442.30	96752
N I	7468.31	96752
N I	8184.85	95533
N I	8188.01	95495
N I	8216.32	95533
N I	8223.12	95477
N I	8242.37	95495
N I	8567.74	97806
N I	8590.01	97770
N I	8629.24	97806
N I	8655.87	97770
N I	8691.6 m	94839
N I	8680.27	94883
N I	8683.40	94832
N I	8686.16	94795
N I	10117 m	104721
O I	7773.4 m	86629
O I	8446.5 m	88631
O I	9263.9 m	97420
Ar I	6965.43	107510
Ar I	7067.22	107260
Ar I	7383.98	107260
Ar I	7503.87	108720
Ar I	7948.18	107100

Ar I	8006.16	106220
Ar I	8103.69	106060
Ar I	8115.31	105490
Ar I	8264.52	107510
Ar I	8408.21	107260
Ar I	8424.65	105570
Ar I	8521.44	107100
Al I	3082.16	32435
Al I	3092.71	32437
Al I	3944.03	25348
Al I	3961.53	25348
Cu I	3247.55	30748
Cu I	3273.96	30535

C The transmission profile of the optical components used

In the figure the optical transmission profiles in the UV-region of the quartz tube, the fused silica lens and the combination of these two components are shown. Material data from the manufactures have been used to calculate the transmission of the specific components. The thickness of the lens has been approximated to be 5 mm.

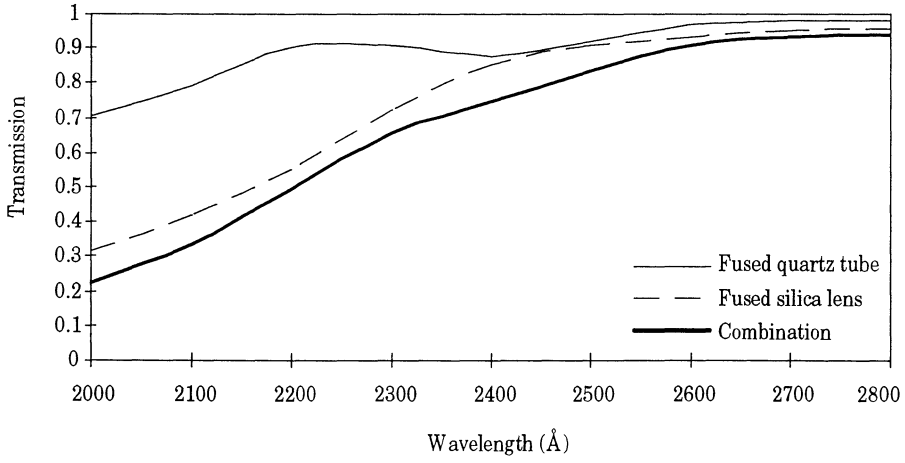

Fig. C.1 *The transmission profiles of the used optical components in the UV-region.*

D Area calculations with OMA vision-PDA software

Intensity area calculations with the OMA vision software were performed to evaluate the total intensity of band systems. It was then noticed that the results obtained with the software were inaccurate. When deriving the intensity of a line (see Eq. (4.1)), the background area, A_{back}, is of no interest. This is illustrated in Fig. D.1, where the line intensity, A_{line}, is obtained by subtracting the background area from the total area. The OMA vision-PDA software, however, when calculating these areas, for some reason divides the total sum of counts, A_{tot}, with a factor of approximately 1.2. The background area is unchanged and, hence, the line area inaccurate. Corrections were made for this error.

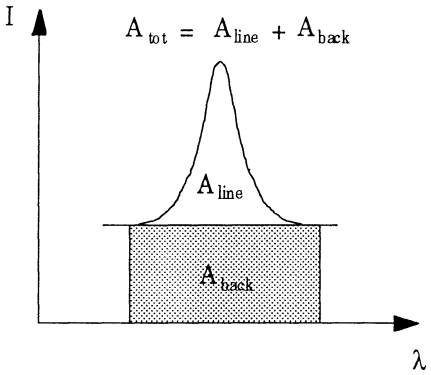

Fig. D.1 *Definition of areas when deriving line intensities.*

E Gas breakdown and steady-state condition[1]

Charged particles are assumed to be created in the gas volume by electron-impact ionization and vanish by recombination at the tube wall, where they arrive by diffusion, D. The probability for ionization is given by the electron-impact ionization frequency $\upsilon(v)$, as a function of the electron velocity v. The continuity equation for the electron density can then be written as

$$\frac{\partial n_e}{\partial t} = \nabla^2(Dn_e) + <\upsilon> n_e . \qquad \text{(E.1)}$$

The diffusion constant generally depends on the electron density, but in the two extremes of low and high n_e, it is density independent and can thus be written as D_e and D_a, respectively. For these two cases we can solve Eq. (E.1) by separating the variables of the density, i.e. we write the electron density as $n_e(\bar{r},t) = \eta(\bar{r})N(t)$. It is now possible, through some calculations, to split the equation into two independent parts, that are set equal to a constant:

$$\frac{\partial}{\partial t}(\eta N) = \nabla^2(D\eta N) + <\upsilon>\eta N \qquad \text{(E.2)}$$

$$\Leftrightarrow$$

1. A more detailed treatment can be found in Ref. [29].

$$\frac{\partial N}{\partial t}\eta = DN\nabla^2(\eta) + <\upsilon>\eta N \tag{E.3}$$

$$\Leftrightarrow$$

$$\frac{1}{N}\frac{\partial N}{\partial t} - <\upsilon> = \frac{D}{\eta}\nabla^2(\eta) \equiv -\tau\,. \tag{E.4}$$

Hence we have the equation system

$$\begin{cases} \dfrac{dN}{dt} = (<\upsilon> - \tau)N \\ \nabla^2\eta = -\dfrac{\tau\eta}{D} \end{cases}. \tag{E.5}$$

We can now define the characteristic diffusion length Λ from the eigenvalue to Eq. (E5b)

$$\frac{1}{\Lambda^2} = \frac{\tau}{D}. \tag{E.6}$$

This gives the Townsend criterion for breakdown

$$<\upsilon> > \frac{D_e}{\Lambda^2}, \tag{E.7}$$

which will lead the electron density to increase rapidly. Once the density has become large enough, $\Lambda >> \lambda_D$, the diffusion becomes, so called, ambipolar. The diffusive motions of electrons and ions are then collective. This interaction, between the charged particles, increases the mean ion transport velocity while considerably slowing down the electron diffusion. This results in the fact that D_a will be smaller than D_e. At steady-state we then have

$$<\upsilon> = \frac{D_a}{\Lambda^2}. \tag{E.8}$$

By comparing this expression with Eq. (E.7), it can bee shown that a smaller electro-magnetic field is required to maintain a plasma, than is needed to cause the breakdown.

F Grotrian diagrams

In this appendix grotrian diagrams for H, He I, N I, O I, Al I and Ar I are presented. The diagrams are taken from Refs. [30,31].

HI GROTRIAN DIAGRAM (1 electron, Z = 1)
(Configuration: nl)
Doublet System

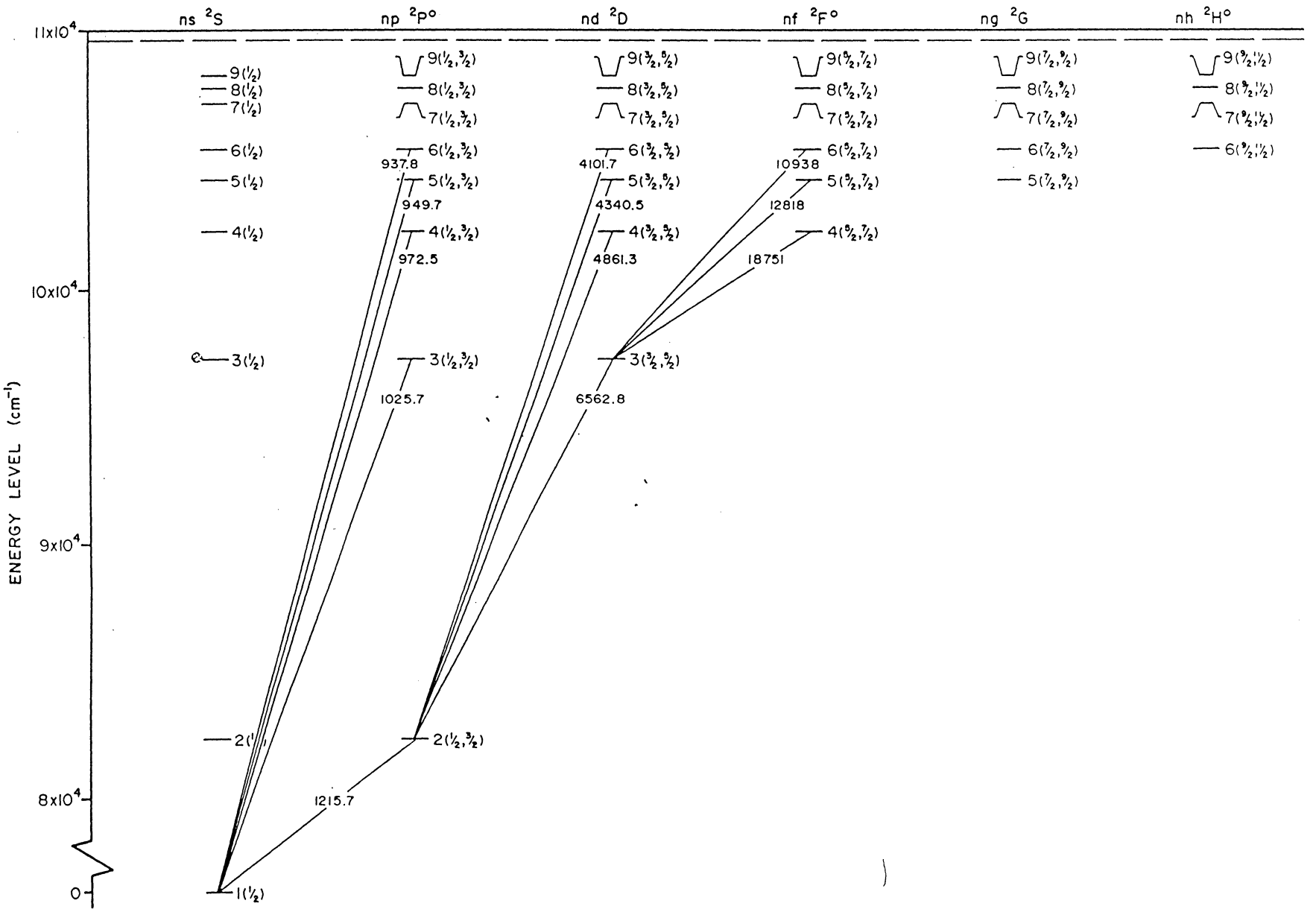

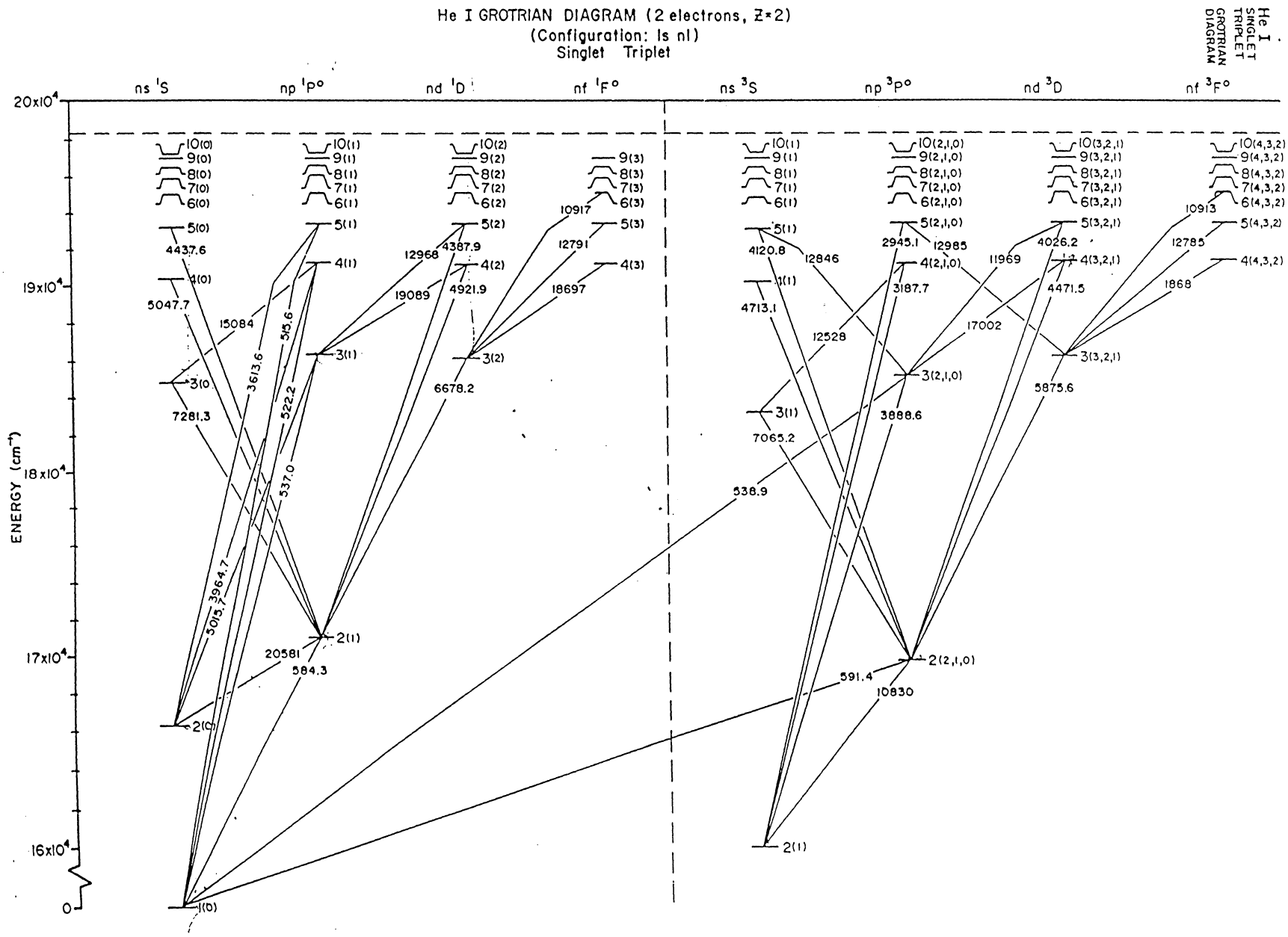
He I GROTRIAN DIAGRAM (2 electrons, Z=2)
(Configuration: 1s nl)
Singlet Triplet
ns 1S
np 1P°
nd 1D
nf 1F°
ns 3S
np 3P°
nd 3D
nf 3F°
ENERGY (cm-1)
20x10^4
19x10^4
18x10^4
17x10^4
16x10^4
0
1(0)
2(0)
2(1)
3(0)
3(1)
3(2)
4(1)
4(2)
5(1)
5(2)
10(0)
9(0)
8(0)
7(0)
6(0)
10(1)
9(1)
8(1)
7(1)
6(1)
10(2)
9(2)
8(2)
7(2)
6(2)
9(3)
8(3)
7(3)
6(3)
5(3)
4(3)
4437.6
5047.7
7281.3
15084
3613.6
515.6
522.2
537.0
5015.7
3964.7
20581
584.3
19089
12968
4387.9
4921.9
6678.2
10917
12791
18697
2(1)
3(1)
4(1)
5(1)
10(1)
9(1)
8(1)
7(1)
6(1)
5(2,1,0)
4(2,1,0)
3(2,1,0)
2(2,1,0)
10(2,1,0)
9(2,1,0)
8(2,1,0)
7(2,1,0)
6(2,1,0)
4120.8
4713.1
7065.2
538.9
12846
3187.7
12528
2945.1
12985
3888.6
591.4
10830
11969
17002
10(3,2,1)
9(3,2,1)
8(3,2,1)
7(3,2,1)
6(3,2,1)
5(3,2,1)
4(3,2,1)
3(3,2,1)
4026.2
4471.5
5875.6
10913
12785
1868
10(4,3,2)
9(4,3,2)
8(4,3,2)
7(4,3,2)
6(4,3,2)
5(4,3,2)
4(4,3,2)
He I
SINGLET
TRIPLET
GROTRIAN
DIAGRAM

NI GROTRIAN DIAGRAM (7 electrons, Z=7)
(Configuration: $1s^2 2s^2 2p^2 nl$, Quartet and Sextet Systems)

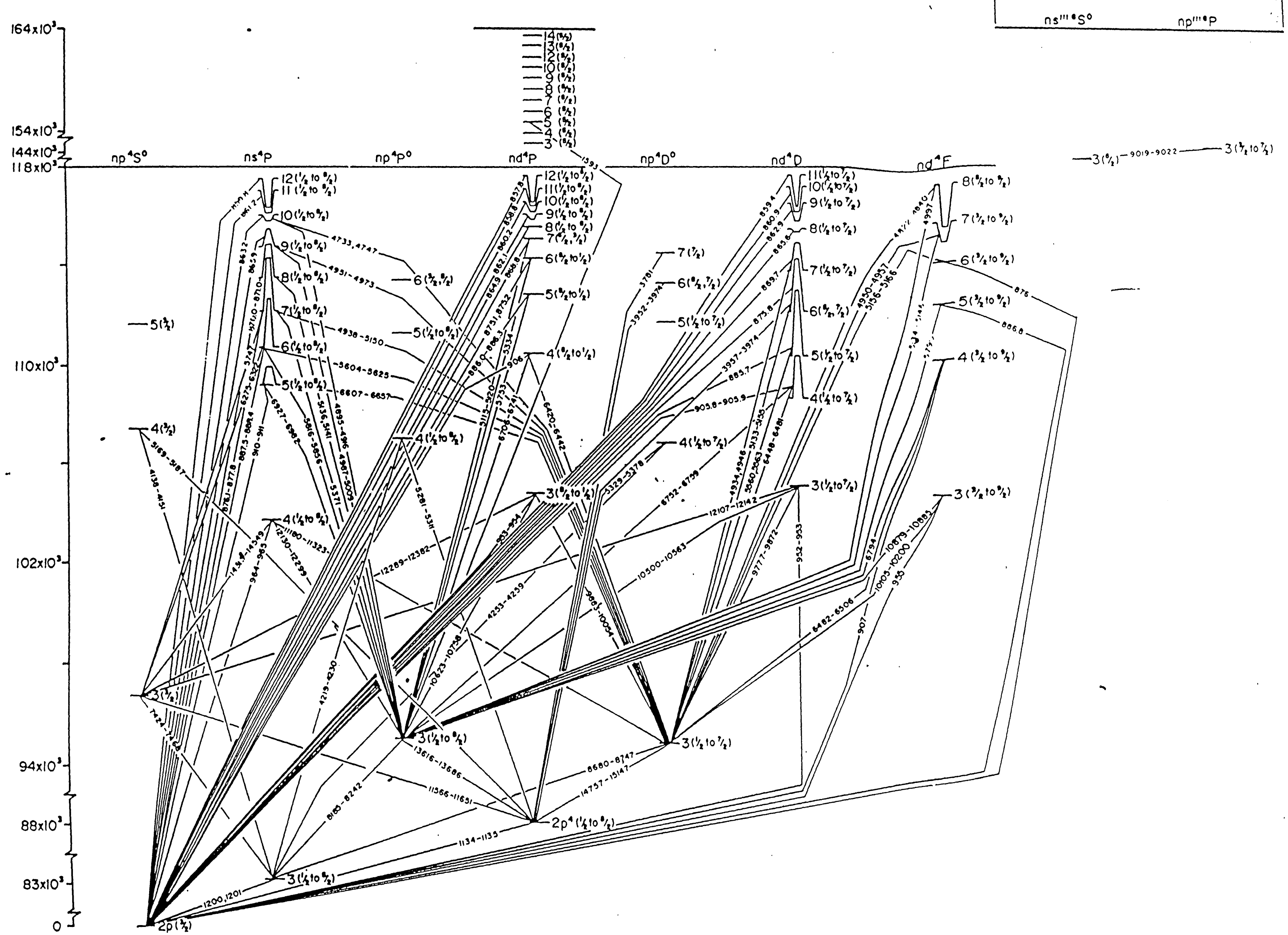

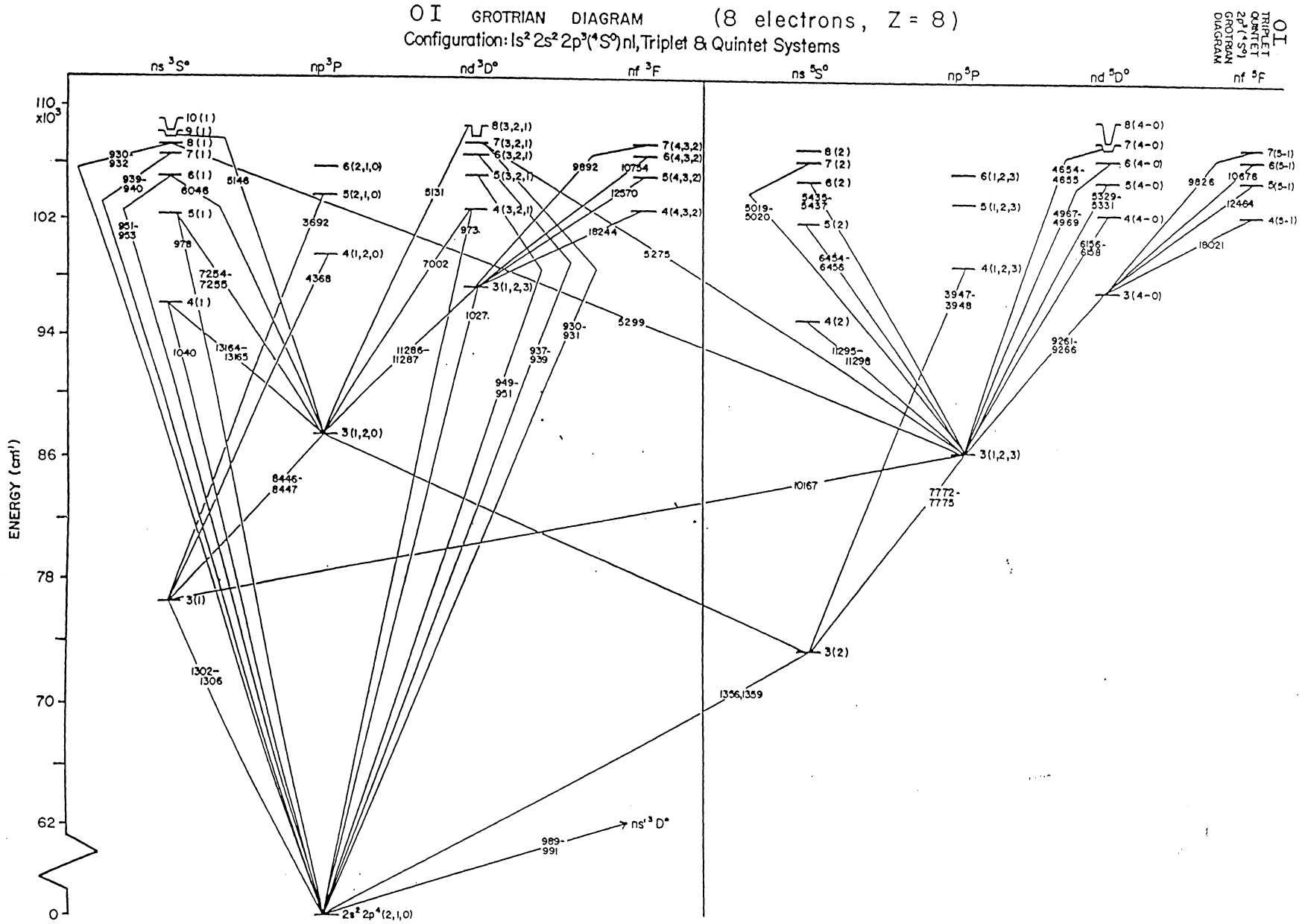
O I GROTRIAN DIAGRAM (8 electrons, Z = 8)
Configuration: 1s² 2s² 2p³(⁴S°)nl, Triplet & Quintet Systems
ns ³S°
np ³P
nd ³D°
nf ³F
ns ⁵S°
np ⁵P
nd ⁵D°
nf ⁵F
ENERGY (cm⁻¹)
110 x10³
102
94
86
78
70
62
0
10(1)
9(1)
8(1)
7(1)
6(1)
5(1)
4(1)
3(1)
930-932
939-940
951-953
978
1040
1302-1306
6048
5146
13164-13165
6(2,1,0)
5(2,1,0)
4(1,2,0)
3(1,2,0)
3692
4368
8446-8447
8(3,2,1)
7(3,2,1)
6(3,2,1)
5(3,2,1)
4(3,2,1)
3(1,2,3)
5131
973.
7002
11286-11287
1027.
949-951
937-939
930-931
9892
10754
12570
18244
7(4,3,2)
6(4,3,2)
5(4,3,2)
4(4,3,2)
5275
3299
8(2)
7(2)
6(2)
5(2)
4(2)
5019-5020
5433-5437
6454-6456
11295-11298
6(1,2,3)
5(1,2,3)
4(1,2,3)
3(1,2,3)
3947-3948
10167
7772-7775
1356,1359
3(2)
8(4-0)
7(4-0)
6(4-0)
5(4-0)
4(4-0)
3(4-0)
4654-4655
4967-4969
5329-5331
6156-6158
9261-9266
9826
10676
12464
18021
7(5-1)
6(5-1)
5(5-1)
4(5-1)
989-991
ns' ³D°
2s² 2p⁴(2,1,0)
O I TRIPLET QUINTET 2p⁴(¹S°) GROTRIAN DIAGRAM

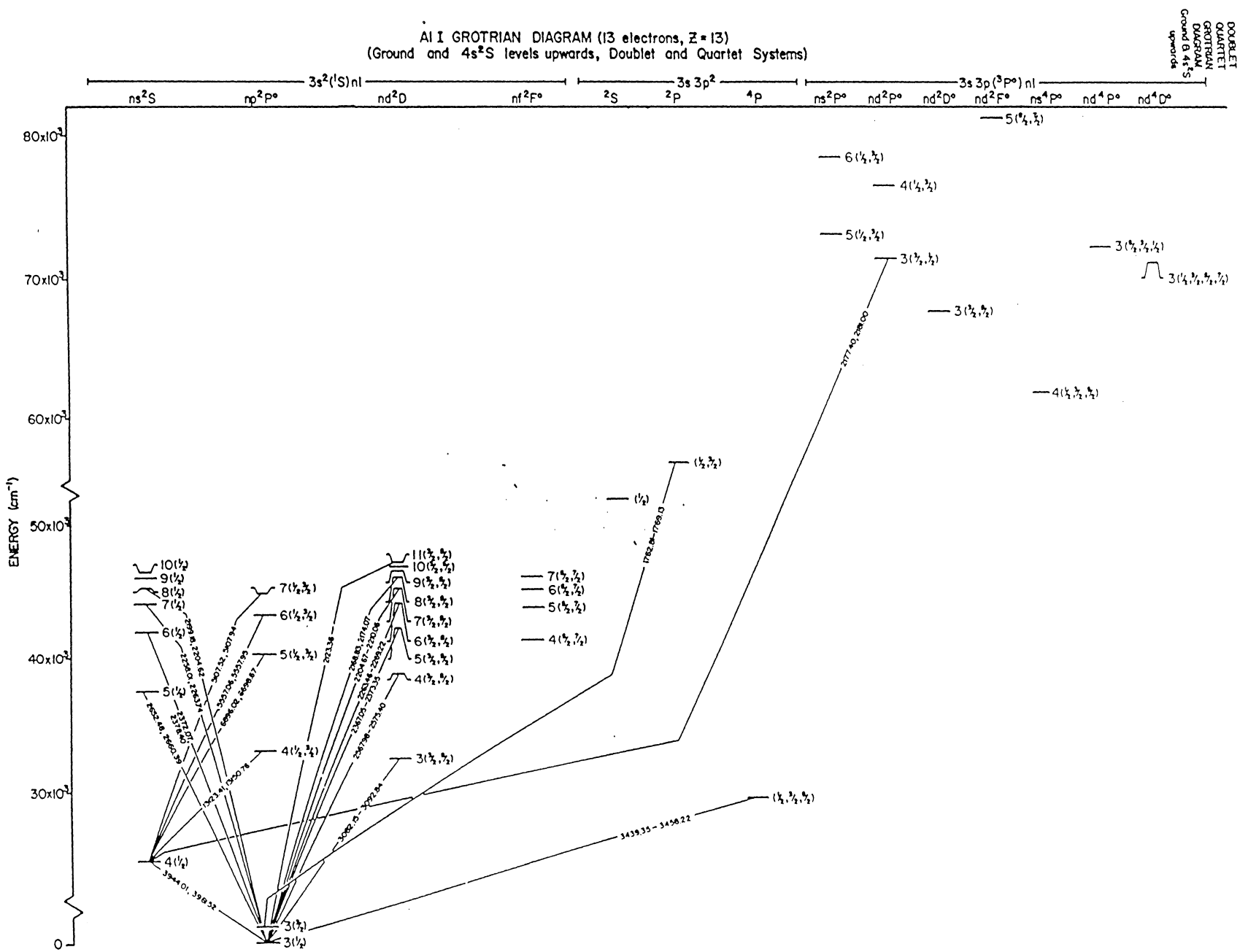
Al I GROTRIAN DIAGRAM (13 electrons, Z = 13)
(Ground and 4s²S levels upwards, Doublet and Quartet Systems)
Al I
DOUBLET QUARTET GROTRIAN DIAGRAM
Ground & 4s²S upwards
3s²(¹S)nl
3s 3p²
3s 3p(³P°) nl
ns²S
np²P°
nd²D
nf²F°
²S
²P
⁴P
ns²P°
nd²P°
nd²D°
nd²F°
ns⁴P°
nd⁴P°
nd⁴D°
ENERGY (cm⁻¹)
80x10³
70x10³
60x10³
50x10³
40x10³
30x10³
0

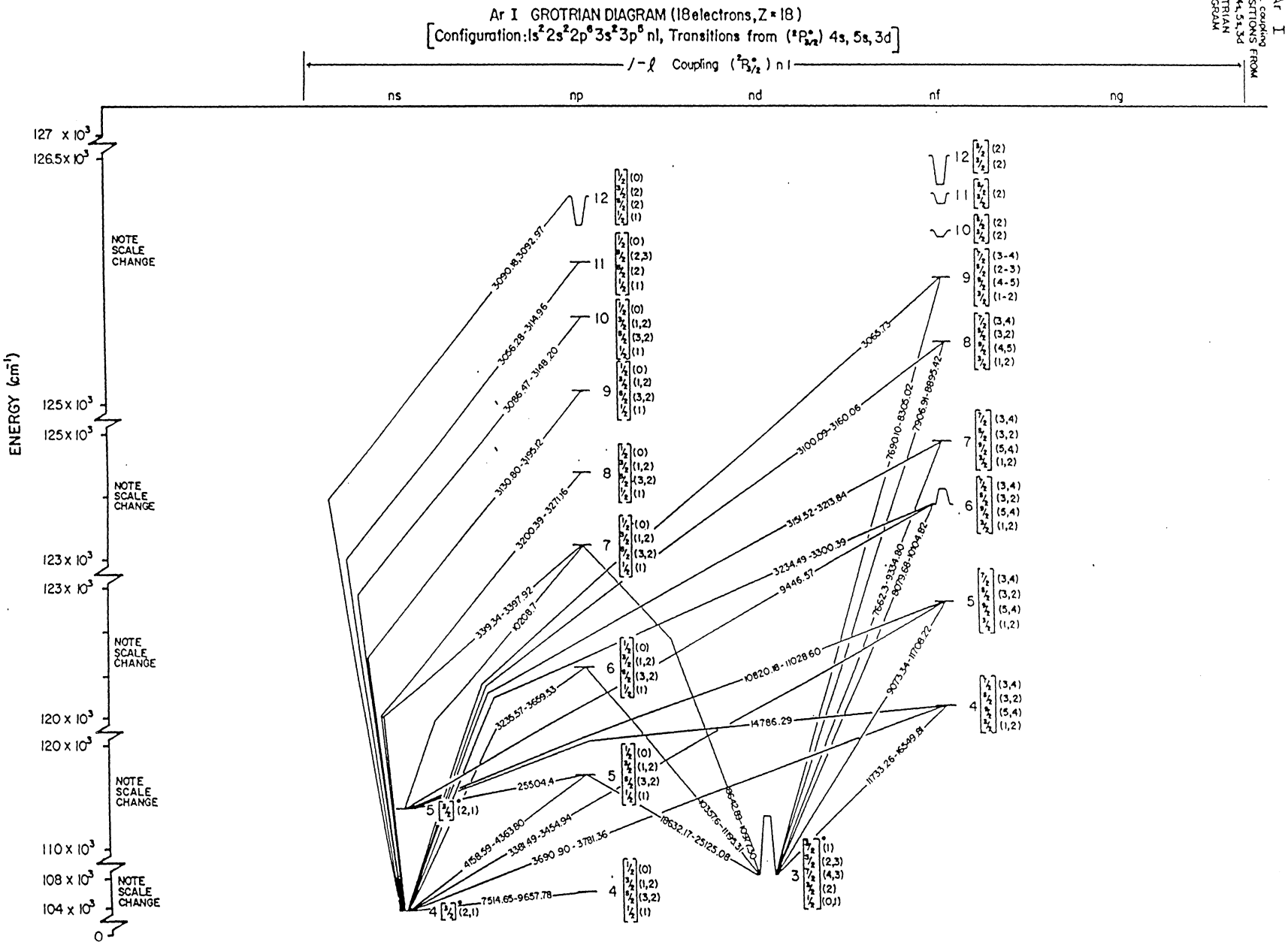
Ar I GROTRIAN DIAGRAM (18 electrons, Z = 18)
[Configuration: 1s² 2s² 2p⁶ 3s² 3p⁵ nl, Transitions from (²P°3/2) 4s, 5s, 3d]
j-l Coupling (²P°3/2) nl
ns
np
nd
nf
ng
ENERGY (cm⁻¹)
127 x 10³
126.5x 10³
125x 10³
125x 10³
123x 10³
123x 10³
120 x 10³
120 x 10³
110 x 10³
108 x 10³
104 x 10³
0
NOTE SCALE CHANGE
Ar I
j-l coupling TRANSITIONS FROM (²P°3/2) 4s, 5s, 3d GROTRIAN DIAGRAM